การกำจัดกรดแฮโลอะซิติกโดยการดูดติดผิวบนเมโซพอรัสซิลิเกต

นายสุวัฒน์ สูงเลิศส่งฟ้า

REMOVAL OF HALOACETIC ACID BY ADSORPTION
ON MESOPOROUS SILICATES

Mr. Suwat Soonglerdsongpha
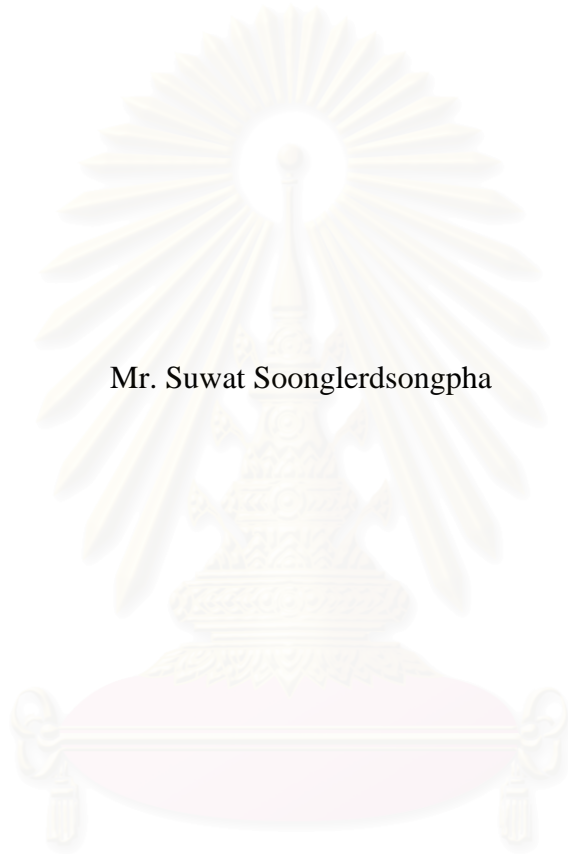
A Thesis Submitted in Partial Fulfillment of the Requirements
for the Degree of Master of Science Program in Environmental Management
(Interdisciplinary Program)
Graduate School
Chulalongkorn University
Academic Year 2006

Thesis Title	REMOVAL OF HALOACETIC ACID BY ADSORPTION ON MESOPOROUS SILICATES
By	Mr. Suwat Soonglerdsongpha
Field of Study	Environmental Management
Thesis Advisor	Patiparn Punyapalakul, Ph.D.
Thesis Co-advisor	Chawalit Ngamcharussrivichai, Ph.D.

Accepted by the Graduate School, Chulalongkorn University in Partial Fulfillment of the Requirements for the Master's Degree

…………………………………………Dean of the Graduate School
(Assistant Professor M.R.Kalaya Tingsabadh, Ph.D.)

THESIS COMMITTEE

………………………………… Chairman
(Manaskorn Rachakornkij, Ph.D.)

…………………………………………Thesis Advisor
(Patiparn Punyapalakul, Ph.D.)

…………………………………………Thesis Co-advisor
(Chawalit Ngamcharussrivichai, Ph.D.)

…………………………………………Member
(Punjaporn Weschayanwiwat, Ph.D.)

………………………………… Member
(Assistant Professor Khemarath Osathaphan, Ph.D.)

สุวัฒน์ สูงเลิศส่งฟ้า : การกำจัดกรดแฮโลอะซิติกโดยการดูดติดผิวบนเมโซพอรัสซิลิเกต. (REMOVAL OF HALOACETIC ACID BY ADSORPTION ON MESOPOROUS SILICATES) อ. ที่ปรึกษา : อ. ดร. ปฏิภาณ ปัญญาพลกุล, อ. ที่ปรึกษาร่วม : อ. ดร. ชวลิต งามจรัสศรีวิชัย, 82 หน้า.

กรดแฮโลอะซิติกเป็นผลผลิตพลอยได้จากการเติมคลอรีน เพื่อฆ่าเชื้อโรคในกระบวนการผลิตน้ำประปาซึ่งสารบางตัวจัดเป็นสารก่อมะเร็ง งานวิจัยนี้ศึกษาถึงการกำจัดกรดแฮโลอะซิติกโดยกระบวนการดูดติดผิวบนเมโซพอรัสซิลิเกตและซีโอไลต์เปรียบเทียบกับถ่านกัมมันต์แบบผง โดยกรดไดคลอโรอะซิติกถูกใช้เป็นตัวแทนเพื่อศึกษาถึงความสามารถในการดูดซับของวัสดุ จากผลการทดลองพบว่าสมบัติทางกายภาพไม่มีผลกระทบต่อความสามารถในการดูดซับ ยกเว้นประจุและชนิดของหมู่ฟังก์ชันบนพื้นผิว จากแบบจำลองจลนศาสตร์ของการดูดซับอธิบายได้ว่ากลไกการดูดซับกรดไดคลอโรอะซิติกเป็นปฏิกิริยาอันดับสอง นอกจากนี้พบว่าความชอบน้ำมีผลต่อความสามารถในการดูดซับกรดไดคลอโรอะซิติกมากกว่าแรงดึงดูดระหว่างประจุและโครงสร้างของผลึก ความสามารถในการดูดซับกรดไดคลอโรอะซิติกอธิบายได้ดีในแบบจำลองของฟรุนด์ลิชมากกว่าแลงเมียร์ จากผลการศึกษาถึงผลของ pH และอุณหภูมิ พบว่า ความสามารถในการดูดซับกรดไดคลอโรอะซิติกขึ้นอยู่กับ pH_{ZPC} ของตัวดูดซับ การดูดซับของกรดไดคลอโรอะซิติกบนถ่านกัมมันต์แบบผงเป็นกระบวนการดูดซับทางกายภาพ ซึ่งตรงข้ามกับการดูดซับบนซีโอไลต์ที่เป็นการดูดซับทางเคมี นอกจากนี้พบว่าอุณหภูมิไม่มีผลกระทบต่อความสามารถในการดูดซับกรดไดคลอโรอะซิติกบนเมโซพอรัสซิลิเกตและแอคติเวทเต็ดอะลูมินา จากการทดลองสามารถสรุปได้ว่า เมโซพอรัสซิลิเกตมีความสามารถในการดูดซับน้อยกว่าถ่านกัมมันต์แบบผง เนื่องจากความซับซ้อนของหมู่ฟังก์ชันบนพื้นผิวของถ่านกัมมันต์แบบผงส่งผลให้เกิดแรงในการดูดซับมากกว่าเมโซพอรัสซิลิเกต

สาขาวิชา การจัดการสิ่งแวดล้อม   ลายมือชื่อนิสิต...สุวัฒน์...สูงเลิศส่งฟ้า...

ปีการศึกษา 2549   ลายมือชื่ออาจารย์ที่ปรึกษา...ปฏิภาณ ปัญญาพลกุล...

ลายมือชื่ออาจารย์ที่ปรึกษาร่วม...

488 95229 20 : MAJOR   ENVIRONMENTAL MANAGEMENT
KEY WORD : HALOACETIC ACID / MESOPOROUS SILICATES / HMS / FUNCTIONALIZED HMS / ADSORPTION.

SUWAT SOONGLERDSONGPHA : REMOVAL OF HALOACETIC ACID BY ADSORPTION ON MESOPOROUS SILICATES. THESIS ADVISOR : PATIPARN PUNYAPALAKUL, Ph.D., THESIS CO-ADVISOR : CHAWALIT NGAMCHARUSSRIVICHAI, Ph.D., 82 pp.

Haloacetic acids are disinfection by-products generated from reaction of chlorine with natural organic matter. Some of them are suspected human carcinogens such as dichloroacetic acid (DCAA). Adsorption of DCAA at low concentration was studied in batch experiment. Synthesized hexagonal mesoporous silicate (HMS) and functionalized HMSs were used to evaluate the effect of surface functional groups compared with powdered activated carbon (PAC) and activated alumina. NaY and HY zeolite were selected to evaluate the effect of crystalline structure. The results showed that physical characteristic of adsorbents did not affect DCAA adsorption capacity, except for surface charge and surface functional groups. The pseudo-second-order kinetic model provided the best correlation of experimental data compared to the pseudo-first-order model. Adsorption capacity suggested that hydrophilicity of adsorbents played more important role than electrostatic force and crystalline structure. Adsorption data were well described by Freundlich isotherm by non-linear estimation. The effects of pH and temperature were also studied. DCAA adsorption capacity was significantly affected by pH depending on pH_{ZPC} of adsorbents. DCAA adsorption capacity on PAC was decreased by increasing of temperature. The opposite result was observed on NaY zeolite. The DCAA adsorption capacity was not affected by temperature significantly for HMS and activated alumina. Therefore, DCAA adsorption capacity of HMS was less than PAC according to several interaction forces involved caused by surface complexity of PAC.

Field of study Environmental Management   Student's signature. Sunat Soonglerdsongpha

Academic year 2006   Advisor's signature. P. RL

                                          Co-advisor's signature. Chawalit N.somichai

ACKNOWLEDGEMENTS

First of all, I would like to express my thankfulness to my advisor, Dr. Patiparn Punyapalakul, for his supervision and helpful suggestion throughout this thesis. I am also grateful to my co-advisor, Dr. Chawalit Ngamcharussrivichai for his suggestive and valuable advice. I would like to take this opportunity to thank Dr. Manaskorn Rachakornkij, chairman of the committee, Dr. Punjaporn Weschayanwiwat and Dr. Khemarath Osathaphan, my committee members, for their useful and valuable comments.

I express my gratitude to the National Research Center for Environmental and Hazardous Waste Management (NRC-EHWM) for providing my tuition and research grants.

My cordial thanks should be given to all the NRC-EHWM staffs and laboratory staffs for their kind cooperation and help.

Additionally, I would like to thank Mr. Theeradit, Mr. Manob, Ms. Dowjai and Mr. Uthai for their assistance in sample analysis.

Finally, I would like to express my sincere gratitude to my beloved family and friends for their love, understanding and heartfelt support.

CONTENTS

LIST OF TABLES

Figure   **Page**

ABBREVIATIONS

HAAs	=	Haloacetic acids
THMs	=	Trihalomethanes
USEPA	=	United State Environmental Protection Agency
MCL	=	Maximum contaminant level
MCAA	=	Monochloroacetic acid
DCAA	=	Dichloroacetic acid
TCAA	=	Trichloroacetic acid
MBAA	=	Monobromoacetic acid
DBAA	=	Dibromoacetic acid
BCAA	=	Bromochloroacetic acid
BDCAA	=	Bromodichloroacetic acid
DBCAA	=	Dibromochloroacetic acid
TBAA	=	Tribromoacetic acid
DBP	=	Disinfection byproduct
NOM	=	Natural organic matters
RO	=	Reverse osmosis
UV	=	Ultraviolet
POU	=	Point of use
GAC	=	Granular activated carbon
PAC	=	Powdered activated carbon
BAC	=	Biological activated carbon
HMS	=	Hexagonal mesoporous silicates
SF-HMS	=	Single-functional hexagonal mesoporous silicates
BF-HMS	=	Bi-functional hexagonal mesoporous silicates
A-HMS	=	Amino functionalized hexagonal mesoporous silicates
M-HMS	=	Mercapto functionalized hexagonal mesoporous silicates
A3M7	=	Combination of amino and mercapto functionalized hexagonal mesoporous silicates at ratio of 3:7
A5M5	=	Combination of amino and mercapto functionalized hexagonal mesoporous silicates at ratio of 5:5

A7M3	=	Combination of amino and mercapto functionalized hexagonal mesoporous silicates at ratio of 7:3
TEOS	=	Tetraethylorthosilicate or tetraethoxysilane
MPTMS	=	Mercaptopropyltrimethoxysilane
APTES	=	Aminopropyltriethoxysilane
M41S	=	Ordered mesoporous molecular sieve, number 41
MCM-41	=	Mobil catalytic material, number 41
CMC	=	Critical micelle concentration
SBUs	=	Secondary building units
CEC	=	Cation exchange capacity
XRD	=	X-ray diffraction
BET	=	Brunauer-Emmett-Teller
BJH	=	Barrett-Joyner-Halenda
FT-IR	=	Fourier transform Infrared
TN	=	Total nitrogen content
ICP-AES	=	Inductively coupled plasma atomic emission
GC-ECD	=	Gas chromatography with electron capture detector
MTBE	=	Methyl-tert-butyl-ether

CHAPTER I
INTRODUCTION

1.1 General

Haloacetic acids (HAAs) are a result of the disinfection process. They form when a chlorine containing disinfectant reacts with natural organic matter (NOM) such as humic acids commonly found in raw water supplies. There are nine species of HAAs (HAA9) occurred in environment. The U.S. Environmental Protection Agency (USEPA, 2001) has regulated the total maximum contaminant level (MCL) in drinking water of five HAAs (HAA5) including Monochloro-, Dichloro-, Trichloro-, Monobromo- and Dibromoacetic acid (MCAA, DCAA, TCAA, MBAA and DBAA) to be less than 60 µg/l in stage 1 and less than 30 µg/l in stage 2.

HAAs at short-term exposure levels above the MCL may increase the chance of spontaneous abortions in pregnant women, but evidence is inconclusive. At long term exposure levels above the MCL, HAAs may cause an increased risk of cancer (Bureau of reclamation, 2003). The USEPA (1999) has classified DCAA as a probable human carcinogen (Group B2) and TCAA as a possible human carcinogen (Group C) (details are given in Table 1.1).

A tendency of disinfection byproducts (DBP) formation kinetic in simulated distribution system produce more dichloroacetic acid as reaction time progressed (Lewis A. Rossman et al., 2001) and DCAA formation is not as affected by pH (M.J. Rodriguez et al.,2004). Moreover, increased HAAs concentration were still relatively high as boiling time increased and found DCAA were not volatilized or degraded by the boiling process (S.W. Krasner and J.M. Wright, 2005). According to HAAs are a probable health threat, many options have increasing concerned to control HAAs concentration and formation in drinking water and water supply. Removal of NOM as HAAs precursors (e.g. humic acid, fulvic acid, etc.) was the primarily significant on HAAs formation. Reverse osmosis (RO) using a semipermeable membrane and high pressure pump is the interesting option NOM removal but some of dissolved NOM can pass through the membrane and high cost for installation this device, in addition, membrane fouling and pretreatment still are limitations. Additionally, using new disinfectants which do not produce disinfection by-product is a motivating option.

Chloramines are the firstly new disinfectant to instead of chlorine because they produce a very low HAA formation nevertheless they can not maintain constant chlorine residual in distribution system up to end of pipe. Ozonation and Ultraviolet (UV) disinfection process have discovered that they can be effective in HAAs reduction conversely they are expensive and also require chlorine residual in distribution system like chloramines (Bureau of Reclamation, 2003).

Table 1.1: The scheme for categorizing chemicals according to their carcinogenic potential

Group A: Human carcinogen	Sufficient evidence in epidemiologic studies to support casual association between exposure and cancer
Group B: Probable human carcinogen	Limited evidence in epidemiologic studies (Group B1) and/or sufficient evidence from animal studies (Group B2)
Group C: Possible human carcinogen	Limited evidence from animal studies and inadequate or no data in humans
Group D: Not classifiable	Inadequate or no human and animal evidence of carcinogenicity
Group E: No evidence of carcinogenicity for human	No evidence of carcinogenicity in at least two adequate animal tests in different species or inadequate epidemiologic and animal studies

Source: USEPA (1996)

For the reason that these techniques can not achieve required HAAs reduction and have more limitations, HAAs removal at end of pipe is still an essential solution. Korshin et al. (2001) studied electrochemical reduction of HAAs by electrochemical treatment. All HAAs were exhibited to be electrochemical active excluding monochloroacetic acid could not be treated. Home use of tap water, THMs and HAAs can be reduced by passage through activated carbon point of use (POU) devices. All of POU devices studied showed a high removal of THMs (>90%). On the other hand, HAAs can be removed about 60-90%, especially; Dichloroacetic acid had the poorest average removal efficiency (44%) (H.S. Weinberg et al., 2006). Like Tung et al.

studied (2006); HAAs had much lower adsorption capacity than trihalomethanes (THMs) on granular activated carbon (GAC) exclusive of trichloroacetic acid. In company with biological activated carbon (BAC) (Xie and Zhou, 2002 and Wu et al., 2005), the efficiency of HAAs removal was a significantly reduced except only trichloroacetic acid was not completely removed. Moreover, increasing the number of halogen atoms affected on HAAs decreased its degradation rate.

According to their limitations and among the inherent disadvantages of activated carbon are their wide distribution of pore size, heterogeneous pore structure, and low selectivity for adsorption. The recent discovery of mesoporous molecular sieves has simulated a renewed interest in adsorbent and catalyst design (Lee et al., 2001). Hexagonal mesoporous silicate (HMS) having been studied extensively in adsorption and catalytic fields, has mesoscale pore and silanol as surface functional group. Silanol group on HMS surface is expected to have high affinity to high hydrophilic molecules such as HAAs. Moreover, HMS surface can be modified by various methods to enhance specific characteristics (e.g., organic ligand modification). Physical characteristic of synthesized HMSs did not affect DCAA adsorption capacity while a higher amount of surface amino-functional groups on HMS giving a higher positive charge exhibited a higher adsorption capacity of DCAA. In addition a combination of mercapto- and amino-functional groups caused a higher surface complexity and produced more active surface sites for adsorption of DCAA (Punyapalakul P. and Takizawa S., 2004). However, adsorption mechanism caused by complexity of surface functional groups has not been studied yet, especially in low concentration level. Moreover, the effect of crystalline structure of silicate material on adsorption capacity of DCAA is still unclear now. Amorphous, microporous and mesoporous materials were applied in this study as adsorbents. The research addressed to the comparison of HAAs adsorption mechanisms and capacities affected by various surfaces functional groups and crystalline structures at low-level concentration of HAAs.

1.2 Hypotheses

The hypotheses for this study are: *i*) HAAs adsorption efficiency of HMS at low-level concentration can be increased by surface modification with amino functional groups. *ii*) HAAs adsorption efficiency in aqueous phase can be affected by surface functional groups complexity. *iii*) Surface characteristics and crystalline structures, for example, pore structure, surface charge, initial surface accessibility, etc. might affect HAAs adsorption capacity.

1.3 Objectives

The main objective of this study is to investigate the effect of surface characteristics and crystalline structures of silica-based adsorbents on HAAs adsorption capacity. The specific objectives are as follows:

1. To determine the effect of surface modification on HAAs adsorption capacity at low-level concentration.
2. To determine the effect of surface complexity of adsorbents on HAAs adsorption capacity at low-level concentration.
3. To study the effect of crystalline structure, pH, and temperature on HAAs adsorption capacity.
4. To compare HAAs adsorption capacity between HMSs and powdered activated carbon at low-level concentration.

1.4 Scopes of Study

The scope of this thesis contains 5 parts are as follow:

1. A direct co-condensation method was performed for organic functionalization of mesoporous materials by using dodecylamine as a template and tetraethoxysilane (TEOS) as a silica precursor. Mercaptopropyltrimethoxysilane (MPTMS), aminopropyltriethoxysilane (APTES) were used for surface functionalized modification on HMS.

2. The physico-chemical characteristics of adsorbents including surface area, pore structure, pore size, surface charge, and surface functional groups were investigated by measure of nitrogen adsorption-desorption measurement, X-ray diffraction, acid-base titration, FT-IR spectroscopy, and elemental analysis, respectively.

3. Equilibrium contact time for DCAA adsorption was performed by varying contact time from 0 to 72 h under batch conditions with a solution concentration of 100 µg/l and amount of adsorbents of 2 g/l.

4. Adsorption isotherms and mechanisms for DCAA were performed by varying concentration of DCAA solution, pH, and temperature under batch conditions with an amount of adsorbent of 2 g/l. The adsorption isotherm models considered in this experiment were Langmuir and Freundlich types.

5. Concentrations of DCAA were determined by using USEPA method 552.2 which are determination of haloacetic acids and dalapon in drinking water by liquid-liquid extraction, derivatization and gas chromatography with electron capture detection.

CHAPTER II
THEORETICAL BACKGROUNDS

2.1 Haloacetic acids

Chlorine is by far the most widely used disinfectant in drinking water treatment. It is also the disinfectant that forms the greatest variety of known byproducts. Of the known chlorination byproducts, the primary byproducts of concern in drinking water treatment are trihalomethanes (THMs) and haloacetic acids (HAAs).

Formation HAAs occurs at the same time when chlorine reacts with natural organic matter (NOM). It is generally believed that the reaction mechanism leading to the formation of HAAs is enhanced under acidic conditions. Therefore, pH will directly influence HAA formation. Moreover, Dojlido et al. (1999) found that the reaction of HAA formation is highly dependent on temperature. When the temperature was low, the biological production was very slow leading to low concentration of NOM. The HAAs concentration was very low as well. When the temperature was high, the algae blooms occurred and NOM content was very high. The HAAs concentration was high and reached 120 μg/l. Among the HAAs formation, dichloroacetic acid (DCAA) and trichloroacetic acid (TCAA) were found to be the highest concentrations. HAAs in water contain nine species, of which five species (HAA$_5$) are currently regulated by the US Environmental Protection Agency (USEPA) including Monochloro-, Dichloro-, Trichloro-, Monobromo- and Dibromoacetic acid (MCAA, DCAA, TCAA, MBAA and DBAA) (Table 2.1). HAAs are colorless, have a low volatility, dissolve easily in water, and are fairly stable (details are given in Table 2.2).

Table 2.1 DBP rule MCL for HAA$_5$

DBP rule for HAA$_5$	MCL (mg/l)
Stage 1 DBP rule	0.060
Stage 2 DBP rule	0.030

Source: USEPA (2001)

Table 2.2 Properties of haloacetic acids (HAAs)

Compound name	Formula	pK_a	bp. (°C)
Monochloroacetic acid (MCAA)	$ClCH_2COOH$	2.865	187.8
Dichloroacetic acid (DCAA)	$Cl_2CHCOOH$	1.30	194
Trichloroacetic acid (TCAA)	Cl_3CCOOH	0.66	196
Monobromoacetic acid (MBAA)	$BrCH_2COOH$	2.902	157
Dibromoacetic acid (DBAA)	$Br_2CHCOOH$	1.47	128-130
Bromochloroacetic acid (BCAA)	$BrClCHCOOH$	1.39	210-212
Bromodichloroacetic acid (BDCAA)	$BrCl_2CCOOH$	1.09	-
Dibromochloroacetic acid (DBCAA)	$Br_2ClCCOOH$	1.09	-
Tribromoacetic acid (TBAA)	Br_3CCOOH	2.10	245

Source: Daniel C. Harris, Quantitative Chemical Analysis

The relation between presence of HAAs in water and human health has been evaluated by several toxicological and epidemiological studies. HAAs at short-term exposure levels above the MCL may increase the chance of spontaneous abortions in pregnant women, but evidence is inconclusive. At long term exposure levels above the MCL, HAAs may cause an increased risk of cancer (Bureau of reclamation, 2003). The USEPA (1999) has classified DCAA as a probable human carcinogen (Group B2) and TCAA as a possible human carcinogen (Group C).

2.2 Mesoporous Silicate

2.2.1 Synthesis and Formation Mechanism of Mesoporous Silicate

The synthesis of a new family of silicate/aluminosilicate mesoporous materials was disclosed by Mobil scientists in 1992. These materials were first described as 'ordered mesoporous molecular sieve' and collectively designated M41S. The M41S family of mesoporous materials was synthesized using silica source and different organic structure directing agents, e.g., cationic surfactants containing long alkyl chain quaternary ammonium compounds containing 10-20 carbons, often followed with addition of co-surfactants. The mesostructure formation depends on the hydrocarbon chain length of the surfactant tail group, the effect of variation of the surfactant concentration and the additional organic swelling agents. The lowest concentration at surfactant molecules aggregating to form spherical isotropic micelles is called critical micelle concentration (CMC_1). Further increase in the surfactant concentration initiates aggregation of spherical into cylindrical or rod-like micelles (CMC_2). There are three main liquid crystalline phases with hexagonal, cubic, and lamellar structures. So far, the most thoroughly investigated member of this new family is MCM-41 (Mobil Catalytic Material, number 41), which consists of an assemblage of non-intersecting tubular pores. The pore structure is composed of a hexagonal array uniform channel of controlled size. The Mobil researchers proposed synthesis mechanism of mesoporous silicates. In the first way, the $C_nH_{2n+1}(CH_3)_3N^+$ surfactant species organize into lyotropic liquid crystal phase, which can serve as template for the formation of hexagonal MCM-41 structure. Firstly the surfactant micelles aggregate into a hexagonal array of rods, followed by interaction of silicate or aluminate anions present in the reaction mixture with the surfactant cationic head groups. Thereafter condensation of the silicate species occurs, leading to the formation of an inorganic polymeric species. After combusting off the surfactant template by calcination, hexagonally arranged inorganic hollow cylinders are produced. In the second way, the silicate species added to the reaction mixture influence the ordering of the isotropic rodlike micelles to the desired liquid crystal phase (Figure 2.1).
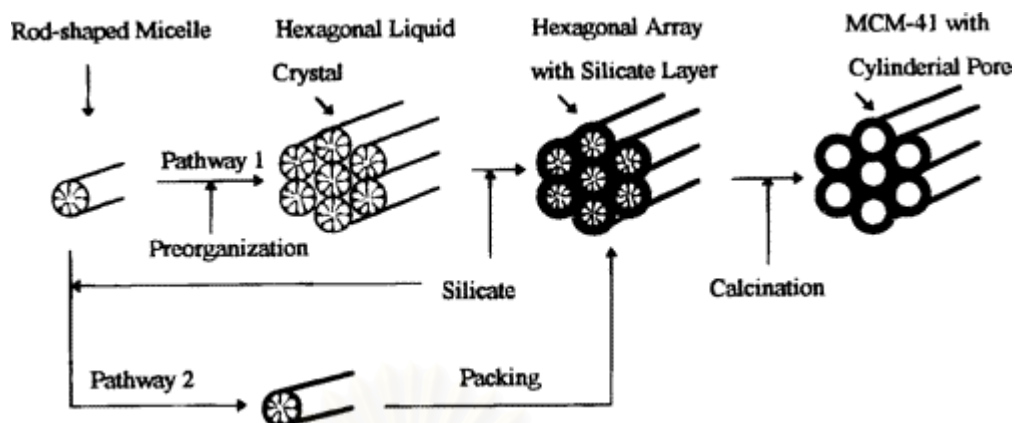
Figure 2.1 Schematic model of liquid crystal templating mechanism via two possible pathways (Beck et al., 1992a).

Tanev and Pinnavaia (1996) proposed Hexagonal mesoporous silicas (HMS) having thicker pore walls, high thermal stability and smaller crystallite size but having higher amounts of interparticle mesoporosity and lower degree of long-range ordering of pores than MCM-41 materials. The formation of neutral HMS mesostructures occurs through the organization of neutral primary amine surfactant molecules (S^0) and neutral $Si(OC_2H_5)_{4-x}(OH)_x$ precursors (I^0) into rodlike assemblies as shown in Figure 2.2. Hydrogen bonding interactions between the precursor silanol hydrogens and the lone electron pairs on the surfactant head groups changes the head-to-chain volume ratio (i.e., the preferred packing) of the surfactant-inorganic complexes and most likely facilitates the assembly of rodlike micelles. Further hydrolysis and condensation of the silanol groups on the micelle-solution interface afford short-range hexagonal packing of the micelles and framework wall formation.
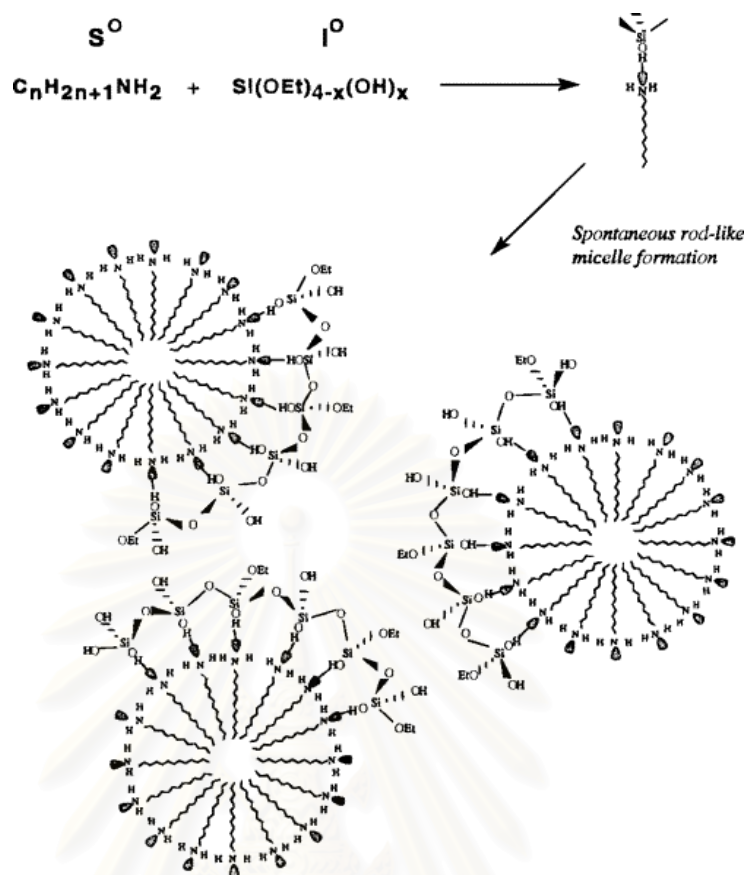
Figure 2.2 Schematic representation of the S^0I^0 templating mechanism of formation of HMS mesoporous molecular sieves. The shaded lobes on the surfactant head groups are electron lone pairs that participate in H bonding with framework silanols. (Tanev and Pinnavaia, 1996)

2.2.2 Organic Functionalization

The application of pure mesoporous silicates or aluminosilicates as catalysts is rather limited because of the limitations in the nature of their active sites. To utilize these mesoporous materials for several specific applications including catalysis and also sorption, ion exchange, sensing etc., the introduction of reactive organic functional groups by modifying the inner surfaces of these materials to form inorganic-organic hybrid is essential. Organically functionalized silicas are a subset of a larger class of hybrid organic-inorganic materials. The covalently bonded organic ligand is usually non-hydrolysable and imparts partial organic character to an inorganic siloxane network. Organic functionalization can be categorized into two general parts:

2.2.2.1 Grafting Method

Grafting refers to post synthesis modification of the inner surface of mesoporous silica, where the organic functional groups are introduced as the terminal groups of an organic monolayer. The large concentration of surface silanol [(-SiO)3Si-OH] groups present in mesoporous silica can be utilized as convenient moieties for anchoring of organic functional groups. The surface modification with organic functional groups is generally carried out by silylation as shown in Figure 2.3.
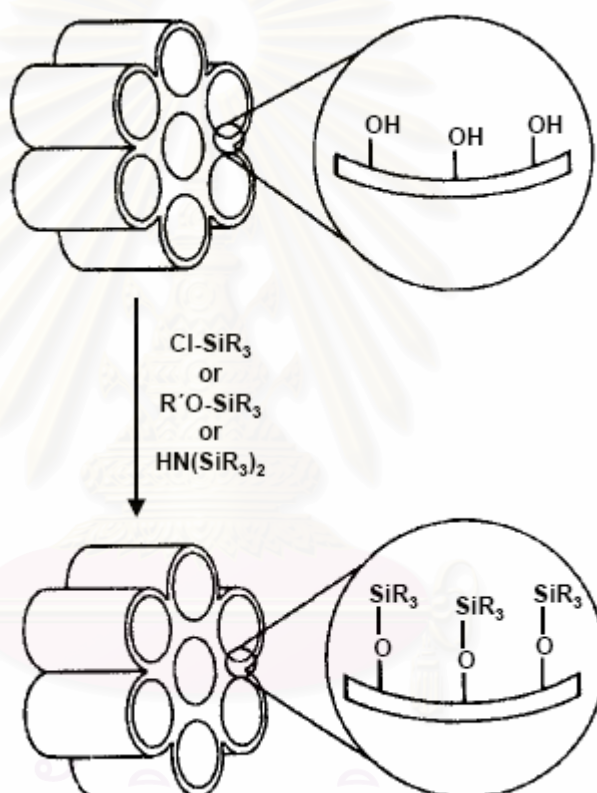
Figure 2.3 Functionalization of inner walls of mesoporous silicates by grafting method. (Stein *et al.*, 2000)

2.2.2.2 Direct Co-Condensation Method

In the grafting methods, incorporation of organic groups is done by attachment of the organosiloxane precursor with surface Si atoms through Si-O-Si-C covalent bond formation. Then Si-O can be cleaved at some reaction conditions. Therefore, in some cases it would be desirable to have direct formation of a C-Si

(surface) covalent bond. Thus, the "one-pot" co-condensation method, where condensation occurs between a tetraalkoxysilane and one or more trialkoxyorganosilanes through sol-gel chemistry (Figure 2.4), seems to have distinct advantages over the grafting methods. A direct co-condensation method is the one-step synthesis of organically functionalized mesoporous silica has two different approaches of synthesis (Mercier and Pinnavaia, 2000) including:

    (1) Template exchange including the replacement of TEOS as well as alkylamine surfactant with organosilane.

    (2) Addition of organosilane by replacing of TEOS with organosilane, maintaining the same alkylamine to TEOS ratio as used to synthesize the non-functionalized HMS materials.

Several research groups have employed this method to prepare inorganic-organic hybrid mesoporous materials under a wide range of synthesis condition. Usually the solvent extraction technique is used to remove the surfactant from the resultant materials.
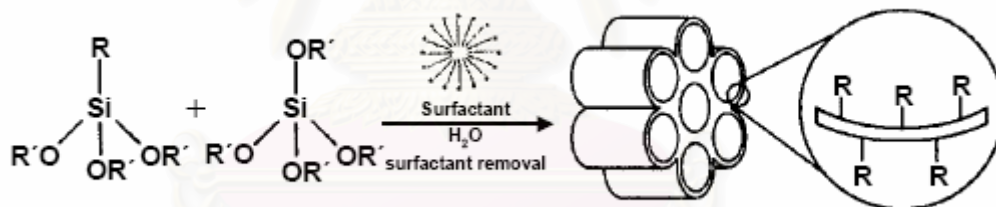
Figure 2.4 Synthesis of organo-functionalized mesoporous silicates by co-condensation. (Stein *et al*., 2000)

2.2.3 Applications of Mesoporous Silicates

Due to the unique physical properties and higher pore sizes than zeolites, mesoporous materials have been highly desirable for catalytic and adsorption applications. Many researchers have studied their properties and tried to develop surface functional groups for more applications. Functionalization of mesoporous materials has played an important role in various aspects such as immobilization of enzymes (Maria Chong and Zhao, 2004, Yiu and Wright, 2005, and Hudson et al.,

2005), development of new catalyst (Aprile et al., 2005), and selective adsorbent (Lee et al., 2001, Newalkar et al., 2003, and Messina et al., 2006). Many functional groups have been studied depending on purpose. Messina and Schulz (2006) modified silica mesoporous materials by TiO_2 for adsorption of reactive dyes. The presence of TiO_2 augmented the adsorption capacities of reactive dyes. They suggested that this would be due to possible degradation of the dye molecule in contact with the TiO_2 particles in the adsorbent interior. Moreover, mesoporous silicates could be grafted on the surface by many organic functional groups to enhance its valuables. Amino-functional group having more hydrophilic than activated carbon has been studied for oxyanion (Yoshitake et al., 2005) and hydrophilic substances adsorption. Moreover, bi-functional mesoporous silica was applied to enhance its settlements. Lee et al. (2001) synthesized bi-functional porous silica (amino- and mercapto- functional groups) for heavy metal ion adsorbent. It could prevent the loss of co-condensed functional groups although hydrothermal stability and heavy metal adsorption capacities decreased introduced by hydrophilicity of amino-functional group. Punyapalakul and Takizawa (2004) developed Hexagonal Mesoporous Silica (HMS) by grafted organic functional group on surface of HMS. The result showed amino-functional group grafted on HMS (A-HMS) had the same adsorption capacity as powder activated carbon (PAC) at high concentration. In addition, combination of amino- and mercapto-functional group which had lower surface charge than amino-functional group had higher adsorption capacity than A-HMS at high concentration.

2.3 Zeolites

Zeolites are microporous crystalline solids with well-defined structures. Generally they contain silicon, aluminium and oxygen in their framework and cations, water and/or other molecules within their pores. Many occur naturally as minerals, and are extensively minded in many parts of the world. Others are synthetic, and are made commercially for specific uses, or produced by research scientists trying to understand more about their chemistry. Because of their unique porous properties, zeolites are used in a variety of applications. Major uses are in petrochemical cracking, ion-exchange (water softening and purification), separation and adsorption.

The basic unit of a zeolitic structure is the TO_4 tetrahedron, where T is normally a silicon or aluminium atom/ion (or phosphorous in an aluminophosphate). The

general formula of the aluminosilicate zeolites is $M_{x/n}[(AlO_2)_x(SiO_2)_y]\cdot mH_2O$. The zeolite framework is composed of $[(Al_2O_3)_x(SiO_2)_y]$ and M is a non-framework, exchangeable cation. The great variety of zeolites is made possible by the different arrangements of linked TO_4 tetrahedra within secondary building units (SBUs), which are linked themselves together in numerous three-dimensional networks. The two simplest SBUs are rings of four and six tetrahedra and others comprise larger single and double ring up to 16 T atoms. The unit cell always contains an integral number of SBUs.
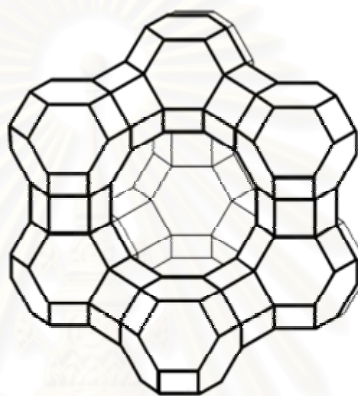
Figure 2.5 Structure of Faujasite-type zeolite

Zeolite Y is the faujasite-type zeolite (Figure 2.5). It has the same framework structure as zeolite X. They crystallize with cubic symmetry. The general composition of the unit cell of faujasite is $(Na, Ca, Mg)_{29}[Al_{58}Si_{134}O_{384}]\cdot 240H_2O$. The SBUs are double six-rings and FD is 12.7 nm^{-3}. The unit cell contains eight cavities, each of diameter $\approx$ 1.3 nm. The three-dimensional channels have 12-ring windows with free apertures of about 0.74 nm. The difference between zeolites X and Y is in their Si/Al ratios which are 1-1.5 and 1.5-3, respectively.

2.4 Activated Alumina

Alumina occurs in nature as corundum, α-Al_2O_3, which is noted for its great hardness, high electrical resistance and low chemical reactivity. It can be made by the heat temperature treatment (at >1200º C) of boehmite or gibbsite and normally has a low specific area (<5 m^2g^{-1}). The activated alumina is generally applied to an adsorbent alumina (usually an industrial product) prepared by the heat treatment of

some form of hydrated alumina (i.e. a crystalline hydroxide, oxide-hydroxide or hydrous alumina gel). It is highly porous and more reactive. Its BET areas are typically 300-400 m^2g^{-1} and it can be used as catalysts and catalyst supports also. Activated alumina was effectively used for the removal of As (III) ions (Singh and Pant, 2003 and Lin and Wu, 2000). The equilibrium was independent of initial As (III) concentration. However, the arsenite removal was strongly dependent on pH and temperature. They found that As (III) ions had high affinity towards activated alumina at pH 7.6. In addition, Ghorai and Pant (2004) studied the removal of fluoride in drinking water by adsorption on activated alumina. It was found that the maximum adsorption takes place at pH value of 7. They suggested that at pH>7, silicates and hydroxyl ions appeared to compete more strongly with fluoride ions for alumina exchange sites and at pH<7, the soluble alumino-fluoro complexes are formed resulting in the presence of aluminium ions in the treated water.

2.5 Activated Carbon (AC)

Activated carbon is made of tiny clusters of carbon atoms stacked upon one another. The carbon source is a variety of materials, such as peanut shells or coal. The raw carbon source is slowly heated in the absence of air to produce a high carbon material. The carbon is activated by passing oxidizing gases through the material at extremely high temperatures. The activation process produces the pores that result in such high adsorptive properties. Most activated carbons are highly microporous. Activated carbon is effective for some contaminants and not effective for others. It does not remove microbes, sodium, nitrates, fluoride, and hardness.

2.6 Adsorption Theory

2.6.1 Mechanism of Adsorption onto Porous Adsorbent

Adsorption is the interphase accumulation or concentration of substances at a surface or interface. Such a process can occur at an interface of any two phases, such as liquid-liquid, gas-liquid, gas-solid, or liquid-solid interfaces. While there is a preponderance of solute (sorbate) molecules in the solution, there are none in the sorbent particle to start with. This imbalance between the two environments amounts

to a driving force for the solute species. First to create a sorbate layer on the surface and then the sorbate may gradually penetrate deeper into the solid. A surface phenomenon in term of adsorption can be distinguished into 2 parts including physical adsorption, is non-specific and the forces attracting the molecules to the solid are relatively weak for example covalent, electrostastic, and van der waals force and chemisorption is specific and involves forces much stronger than in physical adsorption such as chelation of metals.

Many factors influence the adsorptive capacity for specific organic solutes of a homologous series. First, there are the adsorbate properties of group functionality, branching or geometry, polarity, hydrophobicity, dipole moment, molecular weight and size, and aqueous solubility. Second, there are solution conditions such as pH, temperature, adsorbate concentration, ionic strength, and competitive solutes. Third, there is the nature of the adsorbent with its surface area, pore size and distribution of functional groups.

2.6.1.1 Properties of Sorbent Materials

The importance of the surface properties (including sorptive properties) of a given weight of material exposed to solution, increase in proportion to the surface area of that material, and to its surface charge (or site) density or number of charged sites per unit area or weight. Surface charge may be permanent and independent of solution composition, or variable, changing with solution composition. The CEC of the smectite and vermiculite clays and the zeolites is largely permanent and independent of solution chemistry. In contrast, the metal oxyhydroxides and kaolinite clay have a surface charge that is strongly pH-dependent; they are net positive at low pH values and net negative at higher pH values.

The zeolites are a group of hydrated aluminosilicate minerals with open framework structures of (Si, Al)O_4 tetrahedra, charge-balanced mostly by Ca^{2+}, Na^+, or K^+. The isomorphous substitution of tetrahedral Al^{3+} for Si^{4+} creates a negative charge within the cavities. Monovalent and divalent cations in the cavities are weakly held and readily exchangeable. Because cation exchange takes place within the zeolite crystal lattice, it is practically independent of particle size. Since it

results from isomorphous substitution, the CEC of zeolites is permanent and nearly pH-independent.

The surface charge of oxides, hydroxide, phosphate, and carbonates is produced chiefly by ionization of surface groups, or surface chemical reactions. For example, the pH-dependent surface charge of silicate might reflect the presence of surface species written symbolically as $SiOH_2^+$, $SiOH$, and SiO^-. The surface species are positively charged at low pH and deprotonate as pH increases to form neutral and negatively charged species at intermediate and higher pH's, consistent with the amphoteric behavior of the oxide or hydroxide.

2.6.1.2 Properties of Sorbates

The properties and structure of the sorbates most likely to be found in electrostatic attraction are stressed, especially dissociation constant for acid compounds. Acid dissociation constants are commonly reported as pK_a values. Acidity constants of organic compounds depend on the type of functional acid groups. For example, carboxylic acids are significant components of most contaminants originating from organic-rich wastes. They have a range of pK_a values of 1-5 as illustrates in Table 2.1. The high apparent of carboxylate ions occur at higher pH of solution than pK_a, and they will be protonated to form carboxylic acids at lower pH.

Table 2.3 Acid dissociation constants for some carboxylic acids.

Name	Formula	pK_a	K_a
Formic acid	CH_3COOH	3.745	1.80×10^{-4}
Acetic acid	C_2H_5COOH	4.757	1.75×10^{-5}
Chloroacetic acid	$ClCH_2COOH$	2.865	1.36×10^{-3}
Dichloroacetic acid	$Cl_2CHCOOH$	1.30	5.0×10^{-2}
Trichloroacetic acid	Cl_3CCOOH	0.66 (μ=0.1)	0.22

Source: Daniel C. Harris, Quantitative Chemical Analysis

2.6.1.3 Temperature Effect

It was noted that the temperature can influence the sorption process. The binding of Co by the brown alga *Ascophyllum nodosum* increased by 50-70% when the temperature was raised from 4 to 23°C. Temperature increase to 40°C caused only a slight binding increase, whereas temperature of 60°C or more caused a change in the texture of the sorbent and a loss in the sorption capacity due to the material deterioration. For physical adsorption, adsorption heat $\Delta H^0 < 0$, adsorption reaction is exothermic and preferred at lower temperatures. For chemisorption, $\Delta H^0 > 0$, adsorption reaction is endothermic and favored at higher temperatures. However, the effect of temperature is small as compared to other influencing factors.

2.6.1.4 Influence of pH

Of great importance in both cation and anion sorption is the pH value of the solution. However, the optimum pH for anion adsorption is opposite to that of cation sorption. The state of chemically active sites could be changed by the solution pH. For example, in the case of dye with SO_3^- adsorption by chitin, only when chitin amide groups were protonated with a positive charge, the dye could be effectively bound through its anionic sulfate group onto positively charged chitin amide groups. Chromate adsorption by chitosan was enhanced by lowering pH to 5.7 and was relatively independent of pH from pH 2.5 to pH 5.7. The logarithm of the conjugation acid dissociation constants (pK_a) could be one of the key parameters in determination of the optimum pH for charging the sites.

2.6.1.5 Ionic Strength Effect

The influence of ionic strength is significantly affected ion adsorption by the electrostatic attraction. Bjelopavlic et al. (1999) studied the effect of ionic strength on NOM adsorption by activated carbon. From adsorption isotherm studies it was found that, for six of seven carbons, at low surface concentration, increased ionic strength decreased NOM adsorption.

2.6.1.6 Presence of Other Anions

Other sorbable ions in the solution may compete with the contaminants of interest for sorption sites. The binding of the primary is then decreased. For anion sorption, the study of anion exchange established that the selectivity of anion exchanger could be enhanced by the counterion of higher valence, with the smaller (solvated) equivalent volume and greater polarizability, and interacting more strongly with the fixed ionic groups on the matrix and participating least in complex formation with the co-ion. The established affinity is as follows: $SO_4^{2-}>I^->NO_3^->CrO_4^->Br^->SCN^->Cl^->F^-$. Therefore, it would be appropriate to use strong electrolytic Cl^- salts as background for ionic strength control.

2.6.2 Adsorption Kinetic (Eren Z. and Acar F.N., 2007)

2.6.2.1 The pseudo-first-order model

A simple kinetic of sorption is the pseudo-first-order equation of Lagergren expressed in equation 2.1.

$$\frac{dq_t}{dt} = k_1(q_e - q_t) \qquad\qquad 2.1$$

Integrating equation 2.1 and applying the boundary conditions $q_t = 0$ at $t = 0$ and $q_t = q_t$ at $t = t$, gives

$$\ln(q_e - q_t) = \ln q_e - k_1 t \qquad\qquad 2.2$$

Where k_1 = Lagergren rate constant (h^{-1})

$\quad\quad q_e$ = Amounts of DCAA sorbed at equilibrium (h)

$\quad\quad q_t$ = Amounts of DCAA sorbed at time t (h)

2.6.2.2 The pseudo-second-order model

The pseudo-second-order rate expression is used to describe chemisorption involving valency forces through the sharing or exchange of electrons between adsorbent and adsorbate as covalent forces. The rate of pseudo-second-order reaction may be dependent on the amount of solute sorbed on the surface of adsorbent

and the amount sorbed at equilibrium. The kinetic rate equations can be written as equation 2.3.

$$\frac{dq_t}{dt} = k_1(q_e - q_t)^2 \qquad\qquad 2.3$$

Where k_2 is Pseudo-second-order rate constant (g mg^{-1} h^{-1}). Separating the variables in the equation 2.3 gives integrating this for the boundary conditions $t = 0$ to t and $q_t = 0$ to q_t, gives

$$\frac{t}{q_t} = \frac{1}{2k_2 q_e^2} + \frac{t}{q_e} \qquad\qquad 2.4$$

The advantage of using this model is that there is no need to know the equilibrium capacity from the experiments. In addition, the initial adsorption rate can also be obtained from this model as equation 2.5.

$$h = k_2 q_e^2 \qquad\qquad 2.5$$

Where h is the initial sorption rate (mg/(g min)).

2.6.3 Adsorption Isotherm

Sorption isotherms are plot between the equilibrium adsorption capacity (q) and the final equilibrium concentration of the residual sorbate remaining in the solution (C_e). The equilibrium adsorption capacity, q (mg/g), can be calculated with the equation 2.6.

$$q = \frac{(C_0 - C_e)V}{m} \qquad\qquad 2.6$$

Where C_o is the initial concentration (mg/l), C_e is the residual concentration at equilibrium (mg/l), V is the solution volume (l), and m is the adsorbent mass (g).The adsorption isotherm relationship can also be mathematically expressed. Langmuir and Freundlich isotherm are the most commonly used for describing relationship.

2.6.3.1 Langmuir Isotherm

The Langmuir relationship is of a hyperbolic form as shown in equation 2.7:

Langmuir isotherm: $$q = \frac{q_m b C_e}{1 + b C_e}$$ 2.7

The Langmuir relationship can be linearized by plotting either $(1/q)$ vs $(1/C_e)$ or (C_e/q) vs C_e. Where q_m is the maximum adsorption capacity, b is a Langmuir coefficient related to the affinity between the sorbent and sorbate.

The Langmuir isotherm considers sorption as a chemical phenomenon. It was first theoretically examined in the adsorption of gases on solid surfaces. Langmuir constant $b = 1/K$ which is related to the energy of adsorption through the Arrhenius equation. The higher b and the smaller K, the higher is the affinity of the sorbent for the sorbate. q_m can also to interpreted as the total number of binding sites that are available for sorption, and q as the number of binding sites that are in fact occupied by the sorbate ate the concentration C_e.

Although the Langmuir model sheds no light on the mechanistic aspects of sorption, it provides information on uptake capabilities and is capable of reflecting the usual equilibrium sorption process behavior. Langmuir assumed that the forces that are exerted by chemically unsaturated surface atoms (total number of binding sites) do not extend further than the diameter of one sorbed molecule and therefore sorption is restricted to a monolayer.

In the simplest case the following assumptions were made:

a) Fixed number of adsorption sites; at equilibrium, at any temperature and gas pressure a fraction of the surface sites θ is occupied by adsorbed molecules, and the fraction $1-\theta$ is free.

b) All sorption sites are uniform (i.e. constant heat of adsorption)

c) Only one sorbate.

d) One sorbate molecule reacts with one active site.

e) No interaction between sorbed species.

Assumption of a value for the surface area covered per molecule then could allow computation of the active specific surface area of the sorbent using Avogadro's number. As long as its restrictions and limitations are clearly recognized, the Langmuir equation can be used for describing equilibrium conditions for sorption

behavior in different sorbate-sorbent systems, or for varied conditions within any given system.

2.6.3.2 Freundlich Isotherm

The Freundlich isotherm relationship is exponential form as shown in equation 2.8:

Freundlich isotherm: $\qquad q = kC_e^{(1/n)}$ $\qquad\qquad$ 2.8

Where: k and n are Freundlich constants.

The Freundlich relationship is an empirical equation. It does not indicate a finite uptake capacity of the sorbent and can thus only be reasonably applied in the low to intermediate concentration ranges. A simple sorption isotherm indicates that the highest fraction of the sorbate species sorbed is observed at the lowest sorbate concentration, corresponding to the steepest part of the isotherm plot. Such behavior is typical of all dissolved species. Stated differently, the lower concentration of a dissolved substance in water, the greater fraction of it will be sorbed on solids. This behavior is typical of trace organic and inorganic substances at μg/l concentrations or lower. However, it is easier to handle mathematically in more complex calculations (e.g. in modeling the dynamic column behavior) where it may appear quite frequently. Freundlich model can be easily linearized by plotting it in a (log-log) format.

2.6.4 Comparison of Sorption Performance

Performance of sorbing materials often needs to be compared. The simplest case is when there is only one sorbate species in the system. The comparison of single-sorbate sorption performance is best based on a complete single-sorbate sorption isotherm curve. In order for the comparison of two or more sorbents to be 'fair' it must always be done under the same conditions. These may be restricted by the environmental factors under which sorption may have to take place (pH, temperature, ionic strength, etc.).

By performance of the sorbent is usually meant its uptake (q). The sorbents can be compared by their respective q_m values which are calculated from

fitting the Langmuir isotherm model to the actual experimental data (if it fits). This approach is feasible if there exists the characteristic q_{m} sorption performance plateau (the maximum sorbent saturation). A 'good' sorbent that one always looks for would feature a high sorption uptake capacity q_{m}. However, also desirable is a high affinity between the sorbent and sorbate reflected in good uptake values at low concentrations (C_e). This is characterized by a steep rise of the isotherm curve close to its origin. Performance in this region is reflected in the Langmuir coefficient b.

CHAPTER III
MATERIALS AND METHODS

3.1 Materials

1. Dichloroacetic acid 99+% (ACROS ORGANICS)
2. 1,2,3-trichloropropane 99% (ACROS ORGANICS)
3. Dodecylamine 98% (ACROS ORGANICS)
4. Tetraethoxysilane 98% (ACROS ORGANICS)
5. 3-aminopropyltriethoxysilane (Fluka)
6. 3-mercaptopropyltrimethoxysilane (Chisso)
7. Powder activated carbon
8. Activated alumina TECH GRADE (APS Ajax Finechem)
9. NaY zeolite (Tosoh Corporation, Japan)
10. Ethyl alcohol absolute RPE-ACS (CARLO ERBA)
11. Ammonium nitrate
12. Potassium persulfate
13. Potassium nitrate (MERCK)
14. Sodium hydroxide (LAB SCAN)
15. Hydrochloric acid 37%
16. Nitric acid 65%
17. Hydrofluoric acid 40%
18. Sulfuric acid 98% (LAB SCAN)
19. Boric acid
20. Potassium dihydrogenphosphate (Riedel-de Haen)
21. Dipotassium hydrogenphosphate (Riedel-de Haen)
22. Copper II sulfate pentahydrate (CARLO ERBA)
23. Sodium sulfate anhydrous (CARLO ERBA)
24. Sodium hydrogencarbonate ACS for analysis (CARLO ERBA)
25. Methyl-tert-butyl ether GC GRADE (Fluka)

3.2 Preparation of Adsorbents

3.2.1 HMS Synthesis (Punyapalakul P. and Takizawa S., 2004)

Mix 29.6 mol of water with 0.27 mol of dodecylamine and 9.09 mol of ethanol to form as organic template of HMS. Add 1.0 mol of tetraethoxysilane (TEOS) in the mixture and were then mixed under vigorous stirring. The reaction mixture was aged at an ambient temperature for 18 h. The resulting mixture was filtered and air-dried on a glass plate. The product was calcined in air under static condition at 650 ºC for 4 h to remove organic template.

3.2.2 Synthesis of Single-functional HMS (SF-HMS) (Punyapalakul P. and Takizawa S., 2004)

Mix 50 mol of water with 0.25 mol of dodecylamine and 10.25 mol of ethanol to form as organic template of HMS. Add 1.0 mol of tetraethoxysilane (TEOS) in the mixture and were then mixed under vigorous stirring for 30 min. Then 0.25 mol of 3-aminopropyltriethoxysilane (APTES) or 3-mercaptopropyltrimethoxy-silane (MPTMS) was added in the mixture. The reaction mixture was vigorously stirred for 20 h at ambient temperature and the resulting were filtered and air-dried on a glass plate for 24 h. Residual organosilane and organic template were removed by solvent extraction for 72 h with ethanol.

3.2.3 Synthesis of Bi-functional HMS (BF-HMS) (Punyapalakul P. and Takizawa S., 2004)

Mix 50 mol of water with 0.25 mol of dodecylamine and 10.25 mol of ethanol to form as organic template of HMS. Add 1.0 mol of tetraethoxysilane (TEOS) in the mixture and were then mixed under vigorous stirring for 30 min. Then 3-aminopropyltriethoxysilane (APTES) and 3-mercaptopropyltrimethoxysilane (MPTMS) were added in the mixture. The molar ratio of each reactant was shown in Table 3.1. The reaction mixture was vigorously stirred for 20 h at ambient temperature and the resulting were filtered and air-dried on a glass plate for 24 h.

Residual organosilane and organic template were removed by solvent extraction for 72 h with ethanol.

Table 3.1 Molar ratio of APTES and MPTMS

Reactants	A-HMS	A7M3-HMS	A5M5-HMS	A3M7-HMS	M-HMS
APTES	0.25	0.175	0.125	0.075	-
MPTMS	-	0.075	0.125	0.175	0.25

3.2.4 Preparation of activated alumina and NaY zeolite

Activated alumina and NaY zeolite were activated by temperature. They were added on each evaporating dish and place them into incubator. The temperature of incubator was set at 400 ºC at a rate of 1 ºC/min and hold for 3 h.

3.2.5 Preparation of HY zeolite

HY zeolite was prepared by exchanging of sodium ion of NaY zeolite with ammonium ion by adding 1 M ammonium nitrate at the solid to liquid ratio of 1:20. The mixture was stirred at 60 ºC for 2 h. Then, the resulting was filtered and washed with milli-Q water (18.2 MΩ). The experiment was repeated for 2 times. The retentate was dried at 100 ºC for 12 h and calcined at 400 ºC at a rate of 1 ºC/min and hold for 3 h.

3.3 Physico-Chemical Characterization for Adsorbents

3.3.1 Pore Structure

Pore structures of adsorbents were determined by Powder X-ray diffraction (XRD) patterns of synthesized adsorbent. XRD patterns were recorded on Powder Diffractometer; Bruker AXS Model D8 Discover equipped with Cu Kα radiation source in the 2θ range 0.35-6°.

3.3.2 Surface Area and Pore Size

Nitrogen adsorption-desorption isotherms (BET) were measured at 77 K on a Surface area and Porosity Analyzer Micromeritic model: ASAP 2020 version 1.04H. The BET specific surface areas were calculated by using adsorption data in the relative pressure from 0.06 to 0.14. Pore size distributions were calculated from adsorption branches of isotherms using the Barrett-Joyner-Halenda (BJH) formula.

3.3.3 Surface Functional Group

Surface functional groups of prepared HMSs were investigated by Fourier Transform Infrared (FT-IR) Spectroscopy Nicolet Impact 410. KBr was used as the background and sample mixer (KBr : Sample ratio = 10:1). Before measuring, sample was heated at 110°C for reducing the effect of H_2O at 3750 and 3457 cm^{-1}

3.3.4 Elemental Analysis

3.3.4.1 Analysis of Nitrogen content

The amounts of nitrogen in synthesized HMSs were measured by UV adsorption technique. Adsorbents were digested by potassium persulfate ($K_2S_2O_8$) with base condition in autoclave. Chemicals preparations were described as follows:

Mixture of sodium hydroxide (NaOH) and potassium persulfate was prepared by adding 3 g of potassium persulfate in solution of 4 g NaOH in 100 ml. This solution was newly prepared every time. Stock solution (0.1 mg N/ml) for total nitrogen standard curve was prepared by adding 0.722 g of dried potassium nitrate (KNO3) in milli-Q water, and made volume to 1000 ml. HCl (1+500) was prepared by mixing of 1 HClconc in 500 ml of milli-Q water, and HCl (1+16) also was prepared by mixing 1 HClconc in 16 ml of milli-Q water.

Small amount of sample (50 mg) was added to autoclave glass bottle, and then 50 ml of milli-Q water was added. 10 ml of mixture of NaOH and $K_2S_2O_8$ were added into the mixture and autoclaved at 120°C for 30 min. Then sample was filtered and 25 ml of filtrate was taken. After that, 5 ml of HCl (1+16) were added to adjust pH to 2-3 and filled into 50 ml of colorimetric tube. Sample was diluted to 50

ml by milli-Q water. All samples were measured by UV spectrophotometer at 220 nm. Blank was prepared by adding 5 ml of HCl (1+500) into milli-Q water and diluted to 50 ml. Calibration curve was made by following procedure. 10 ml of prepared TN stock solution was taken and diluted ten times to 100 ml. Then 1-15 ml of obtained solution (0.01 mg N/ml) were added to each colorimetric tube and 5 ml of HCl (1+500) was added to each tube. All of tubes were made volume to 50 ml and measured by UV spectrophotometer with same condition. Amount of TN were plotted against UV-absorbance. TN (mg/g) was calculated by the following equation:

$$\text{TN (mg/g)} \quad = \quad \{[a \times (60/25)] / b\}$$

Where a is amount of TN obtained from calibration curve (mg) and b is amount of synthesized adsorbent (g).

3.3.4.2 Analysis of Sulfur content

The synthesized HMSs were digested with 7 ml of HNO_3 65% and 2 ml of HF 40% in Microwave equipment to analyze the amounts of sulfur. Microwave was temperature-programmed at 240°C in 10 minutes and held for 20 minutes. After microwave completion, samples were cooled by air until the solution reached room temperature. HF in solution was removed by adding 10 ml of H_3BO_3 5% before analysis. The amounts of sulfur were analyzed by Inductively Coupled Plasma Atomic Emission Spectroscopy (ICP-AES).

3.3.5 Surface Charge

Acid/base titration of synthesized HMSs, PAC, zeolites, and activated alumina was carried out using 20 ml of adsorbents mixture (2 g/l). Varying amounts of 0.01 M HCl or 0.01 M NaOH solutions were added to a maximum of 9 samples to vary pH of each sample. There was also one sample with no acid or base addition. Each sample was then diluted to a final volume of 25 ml with Milli Q water. The ionic strength was adjusted with NaCl solution at 0.01 M when diluted in 25 ml. Then the samples were shaken in shaking water bath at 25°C for 12 hr. Surface charges were calculated from suspension pH of each sample measured after equilibrating.

3.4 Adsorption Experiments

3.4.1 Adsorption Kinetic

The equilibrium contact time for DCAA adsorption was performed by varying contact time from 0 to 72 h under batch condition at DCAA concentration of 10 μg/l and amount of adsorbent of 2 g/l. The pH of solution was fixed at pH 7 by phosphate buffer. Samples were shaken in shaking water bath at 25°C, 150 rpm. After that they were filtered by filter paper no.42 and the rest of DCAA concentration then were analyzed following USEPA method 552.2.

3.4.2 Adsorption Isotherm

The DCAA adsorption isotherm was performed by varying DCAA concentration from 10 to 300 μg/l under batch condition. The amount of adsorbent is of 2 g/l. Samples were shaken in shaking water bath at 25°C, 150 rpm until equilibrium. After that they were filtered by filter paper no.42 and the rest of DCAA concentration then were analyzed following USEPA method 552.2.

3.4.3 Effect of pH

The effect of pH for DCAA adsorption was performed by varying pH from 5 to 9 under batch condition at DCAA concentration of 60 μg/l and amount of adsorbent of 2 g/l. Samples were shaken in shaking water bath at 25°C, 150 rpm until equilibrium. After that they were filtered by filter paper no.42 and the rest of DCAA concentration then were analyzed following USEPA method 552.2.

3.4.4 Effect of Temperature

The effect of temperature for DCAA adsorption was performed by varying temperature from 15 to 60°C under batch condition at DCAA concentration of 60 μg/l and amount of adsorbent of 2 g/l. The pH of solution was fixed at pH 7 by phosphate buffer. Samples were shaken in shaking water bath at 150 rpm until equilibrium. After

that, they were filtered by filter paper no.42 and the rest of DCAA concentration then were analyzed following USEPA method 552.2.

3.5 Analytical Method

A concentration of DCAA was determined using USEPA method 552.2 which is determination of haloacetic acids and dalapon in drinking water by liquid-liquid extraction, derivatization and gas chromatography with electron capture detection. A 25 ml volume of sample was adjusted pH to less than 0.5 by adding at least 2 ml of concentrated sulfuric acid. A gram of copper II sulfate pentahydrate was quickly added to the solution and shaked until dissolve followed by 7.5 g of sodium sulfate anhydrous. This acidic solution was extracted with 5 ml of methyl-tert-butyl-ether (MTBE) for 30 minutes. The DCAA that has been partitioned into the organic phase was then converted to its methyl ester by addition of acidic methanol followed by warming at 50 ºC for 2 hours. The acidic extract was neutralized by a back extraction with a saturated solution of sodium bicarbonate and the target analyst was measured by gas chromatography using electron capture detector (GC/ECD) Agilent GC6890. A DB-XLB (J&W scientific) fused silica capillary column (30 m x 0.32 mm i.d. x 0.05 μm film thickness) was used for separation. The injector was kept at 250 ºC, splitless mode, 30 sec purge activation time, and 50 pg per component. Helium was used as carrier gas at 45 cm/sec flow rate. The GC oven was temperature-programmed at 50 ºC for 0.5 min and then from 50-200 ºC at a rate of 15 ºC/min, after that the temperature was held constant for 2 min. The detector temperature was maintained at 350 ºC.

CHAPTER IV
RESULTS AND DISCUSSION

4.1 Physico-Chemical Characterization

In this study, HMS and functionalized HMSs with amino- and mercapto-functional groups were synthesized by co-condensation method. Dodecylamine and TEOS were used as organic template and silica precursor, respectively. APTES and MPTMS were used for amino- and mercapto-groups functionalized SF-HMS and BF-HMS. Then organic template was removed by calcination for HMS and solvent extraction for functionalized HMS. After that, physico-chemical characteristics of synthesized HMSs, Zeolites were investigated comparing with PAC. Obtained data were combined with adsorption experiment results for study relationships between physico-chemical characteristics (ca. crystalline structure, surface characteristics, hydrophilicity, surface charges, etc.) and DCAA adsorption phenomenon.

4.1.1 Pore Structure

Figure 4.1 presents the X-Ray Powder Diffraction (XRD) pattern of synthesized HMSs. According to the XRD pattern, synthesized pristine HMS (pure silica HMS) exhibited a strong single diffraction peak at $2\theta = 2.2^o$ and weak peak around 4.3^o as an evidence of the hexagonal crystalline structure, although crystalline structure of prepared HMS was not complete hexagonal crystalline (comparing with other hexagonal crystalline silicate), which should show an XRD pattern consisting of (100), (110), (200) and (210) diffraction for the hexagonal array of typical HMS material. However, XRD pattern of functionalized HMS indicated that crystalline structure was lost by co-condensation method compared with pristine HMS result.

For functionalized HMSs (A3M7, A5M5, and A7M3), the XRD patterns exhibited very broad peak indicating that the mesostructure of functionalized HMSs became disorder. It might be caused by protonation of APTES under acid or neutral condition. Protonated APTES can cross-link with surface silanol groups of silicate species. On the other hand, protonated APTES might play a strong influence on the
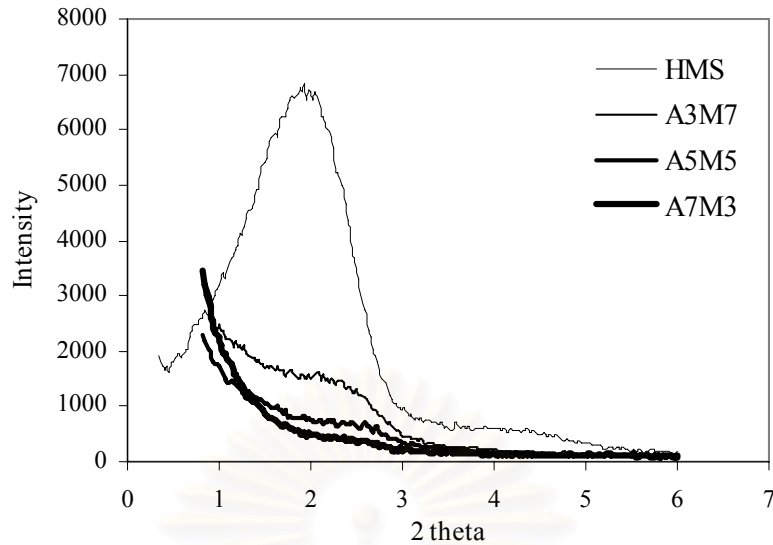
Figure 4.1 XRD patterns of HMS and functionalized HMSs

self assembly of surfactant, leading to weaker interactions of the silicate species with surfactant template (Chong et al., 2004).

4.1.2 Surface Area and Pore Size

The Brunauer-Emmett-Teller (BET) method continues to be the most widely used method for the determination of surface area, pore volumes and pore size distributions of porous materials from nitrogen adsorption-desorption isotherm data. The nitrogen adsorption-desorption isotherms (BET) were measured at 77 K on a Surface area and Porosity Analyzer. The BET equation can be represented in Equation 4.1 as below.

$$\frac{p}{v(p_0 - p)} = \frac{1}{v_m c} + \frac{c-1}{v_m c}\frac{p}{p_0} \qquad 4.1$$

Where v = Volume of N_2 adsorbed by the sample under pressure p

p_0 = Saturated vapor pressure at the same temperature

v_m = Volume of N_2 adsorbed when the surface is covered with a unimolecular layer

and c = Constant for a given adsorbate

The specific surface areas of samples were calculated from the adsorption data by Equation 4.2.

$$S = \frac{N_0 v_m A}{22414m} \qquad 4.2$$

Where S = Specific surface area

N_0 = Avogadro number

m = Amount of solid adsorbent

A = Cross-section of the gas molecules (16.2 $A^{\circ 2}$ for N_2)

The Barrett-Joyner-Halenda (BJH) model was used for calculated of pore size distributions of materials.

The BET surface areas, pore volumes, and pore size distributions of PAC, HMS, functionalized HMSs, NaY, and HY zeolite were shown in Table 4.1.

Table 4.1 BET surface area, pore volume, and pore diameter of PAC, HMS, functionalized HMSs, NaY, and HY zeolite.

Adsorbents	Pore diameter (nm)	BET Surface area (m²/g)	Pore volume (mm³/g)	Surface functional groups
HMS	2.60	712.24	773.42	Silanol
A-HMS	3.95	262.28	147.26	Amino
M-HMS	2.48	912.68	433.47	Mercapto
A3M7-HMS	2.50	482.76	151.98	Amino and Mercapto
A5M5-HMS	2.60	426.40	220.46	Amino and Mercapto
A7M3-HMS	3.58	200.23	186.82	Amino and Mercapto
NaY-Zeolite	0.74	653.13	326.46	Silanol
HY-Zeolite	0.74	370.22	201.61	Silanol
PAC	1.90	980.46	276.00	Carboxyl, Phenyl and others

The BET surface area of PAC, HMS, A-HMS, M-HMS, A3M7, A5M5, A7M3, NaY, and HY zeolite was found to be 980.46, 712.24, 262.28, 912.68, 482.76, 426.40, 200.23, 653.13 and 370.22 m²/g, respectively. The specific surface area of PAC is higher than other adsorbents, that might cause highest adsorption capacity. Furthermore, the results showed that specific surface areas of organosilane functionalized HMSs were decreased due to increasing of amino functional group.

Obviously, amino-functional groups considerably affect the structure of mesoporous silicate which is indicative of decrease of BET surface area. It is aforementioned in XRD patterns that it might be due to cross-link between amino-functional groups and silanol groups of silicates and conduct to weaker interaction between surfactant templates and silicate species. Opposing to amino-functional group, the specific surface area of M-HMS is larger than HMS indicating mercapto-functional groups do not affect disorder of mesostructure.

For pore size distribution, the average pore size of PAC, HMS, A-HMS, M-HMS, A3M7, A5M5, A7M3, NaY and HY zeolite calculated by BJH model was 1.9, 2.60, 3.95, 2.48, 2.50, 2.60, 3.58, 0.74, and 0.74 nm, respectively. PAC has smallest pore size in microporous structure. For HMS and functionalized HMSs, their average pore sizes are in the range of 2-50 nm which indicates that structure of adsorbents are mesoporous structures. However, presence of organo-functional groups on HMS affects to the average pore size. For example, mercaptopropyl groups on M-HMS exhibits a smaller pore size than pristine HMS. However, A-HMS and BF-HMS exhibit the larger average pore size than HMS. It can be concluded that presence of amino-functional groups might deform hexagonal mesostructure which might cause increasing of average pore size. Average pore size of HY zeolite is similar to NaY.

4.1.3 Surface Functional Groups

Surface functional groups of HMS and functionalized HMSs were investigated by Fourier Transform Infrared (FT-IR) Spectroscopy. It deals with the vibration of chemical bonds in a molecule at various frequencies depending on the elements and types of bonds. In this experiment the FT-IR spectra was used to confirm functional groups on adsorbents surface which loaded during synthesis of functionalized HMSs. The FT-IR spectra of HMS and functionalized HMSs were illustrated in Figure 4.2.

Figure 4.2 shows the FT-IR spectra of HMS and functionalized HMSs. All of them exhibit O-H stretching peak at wave number of 3400-3500 cm^{-1}. It indicates that they still have silanol groups on surface of materials. Particularly, HMS shows the highest percent transmittance of FT-IR spectra telling that it has more silanol groups than others. For functionalized HMSs, they express C-H stretching peak at
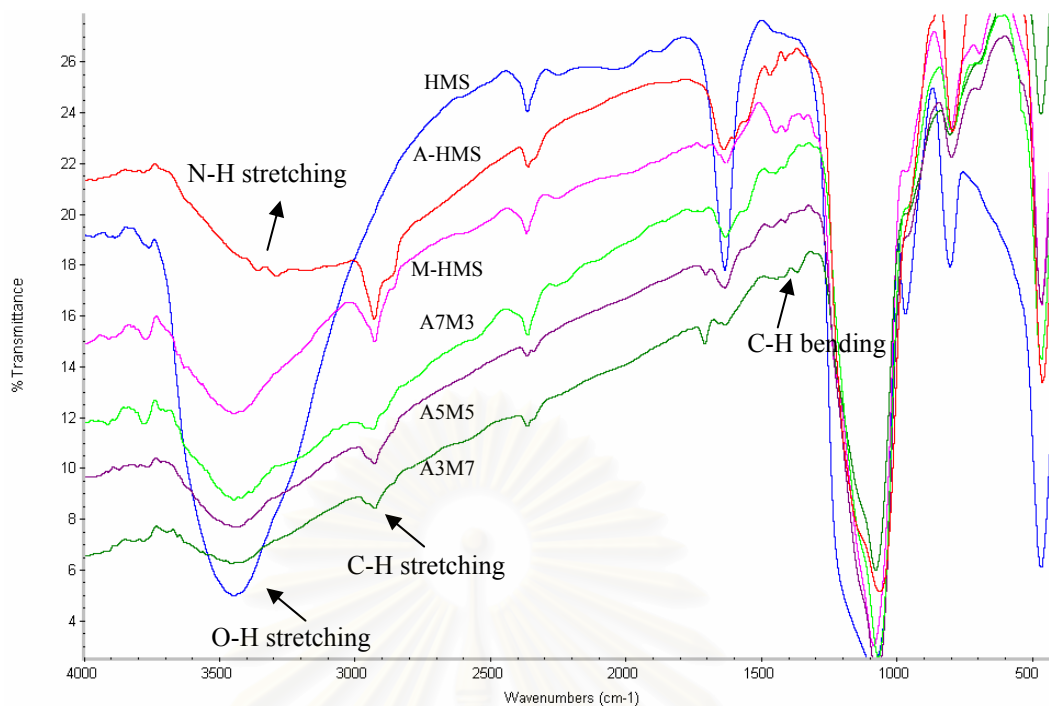
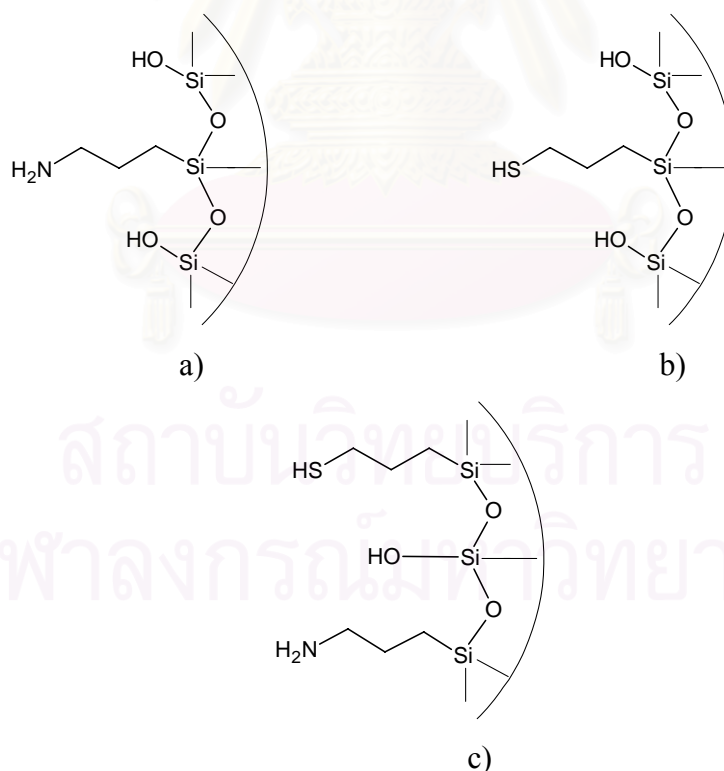**Figure 4.2** FT-IR spectra of HMS and functionalized HMSs

Figure 4.3 Structure of functionalized HMSs a) amino-functionalized HMS b) mercapto-functionalized HMS and c) bi-functionalized HMS

wave number of less than 3000 cm^{-1} and C-H bending of CH$_2$-methylene group at wave number of 1450 cm^{-1}, in spite of disappearance in pristine HMS. The compositions of alkyl group of functionalized HMSs are shown in Figure 4.3.

Moreover, A-HMS exhibits two N-H stretching peak at wave number of 3300-3400 cm^{-1} which indicates the presence of NH$_2$ on surface of HMS. However, it cannot identify mercapto-functional groups (SH) in BF-HMSs. It might be caused by low sensitivity FT-IR spectrophotometer to analyze S-H stretching of mercapto groups.

4.1.4 Elemental Analysis

In addition to the evidences given by FT-IR spectra, amounts of N and S in A-HMS, M-HMS and BF-HMS were investigated for confirming the presence of N and S. Autoclave digestion by potassium persulfate (K$_2$S$_2$O$_8$) in alkaline condition was conducted for quantitative nitrogen analysis. Inductively Coupled Plasma Atomic Emission Spectroscopy (ICP-AES) technique was applied for S quantification. Pure silicate HMS was also investigated as a blank sample. Amount of N in A-HMS was quantified as 1.41%. S in M-HMS was detected as 9.92%. Obtained results and combination with FT-IR spectra of A-HMS and M-HMS can confirmed the presence of amino and mercapto functional groups on the surfaces of A-HMS and M-HMS, respectively.

Nitrogen content of A-HMS, A7M3, A5M5 and A3M7 was found to be 1.41, 1.30, 0.77 and 0.61%, respectively. The result shows that nitrogen content decrease from A-HMS to A3M7. Sulfur content of M-HMS, A3M7, A5M5 and A7M3 was found to be 9.92, 7.09, 5.99 and 3.26%, respectively. The result shows that sulfur contents are nearly equal to amount of MPTMS loaded in synthesis precess. It means that mercapto-functional groups of MPTMS are not affected to reaction between surfactant templates and silica precursor, unlike amino-functional groups of APTES.

Ratios of amino functional groups and mercapto functional groups of BF-HMSs, compared with A-HMS and M-HMS were shown in Figure 4.4. The amount of each functional group of bi-functionally grafted adsorbents can be reconfirmed and were as same as the ratios that were shown in chapter 3.
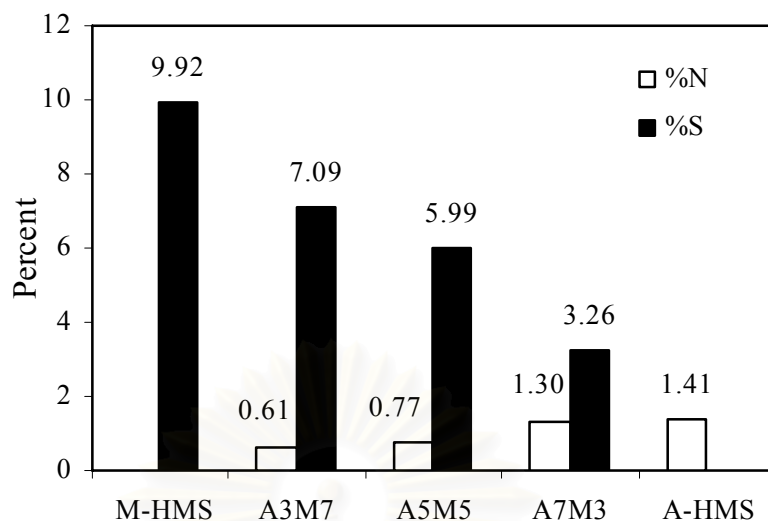
Figure 4.4 Total nitrogen and sulfur content in functionalized HMSs

4.1.5 Surface Charge

Acid/base titration technique was used to determine the surface charge of materials. The ionic strength was fixed at 0.01 M by NaCl solution. After equilibrium, pH of solutions were measured and plotted against surface charges. Surface charges were calculated from the principle of electroneutrality as shown in Equation 4.3.

$$\text{Surface charge (C/g)} = \{[HCl]_{add} - [NaOH]_{add} - [H^+] + [OH^-]\} \times 96500 / W \qquad 4.3$$

Where $[HCl]_{add}$ = Concentration of HCl were added (mol/l)

$[NaOH]_{add}$ = Concentration of NaCl were added (mol/l)

$[H^+]$ = Concentration of proton (mol/l) calculated from

$pH = -log [H^+]$

$[OH^-]$ = Concentration of hydroxide ion (mol/l) calculated

from $pOH = -log [OH^-]$ and $pOH = 14-pH$

96500 = Faraday constant (C/mol)

W = Weight of adsorbent (g/l)

The surface charge density of PAC, HMS, SF-HMSs, BF-HMSs, activated alumina, NaY and HY zeolite as function of pH were shown in Figure 4.5-4.6.
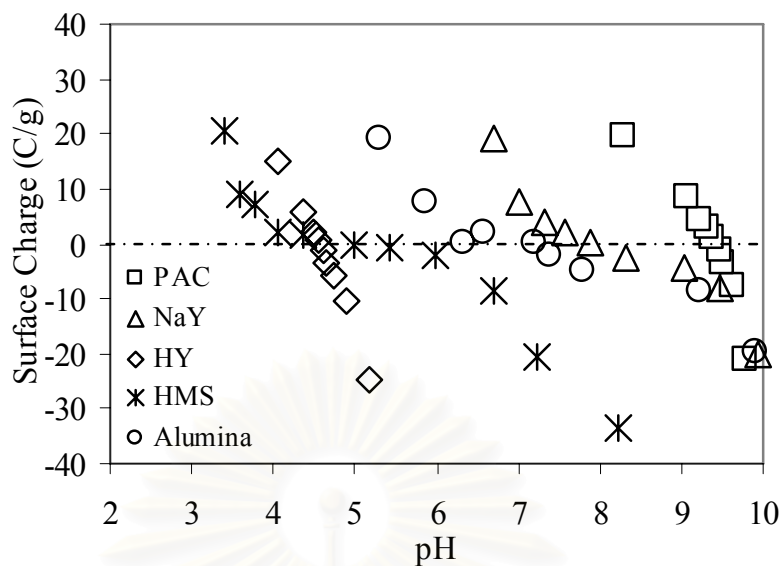
Figure 4.5 Surface charges of PAC, NaY, HY zeolite, HMS and activated alumina as a function of pH
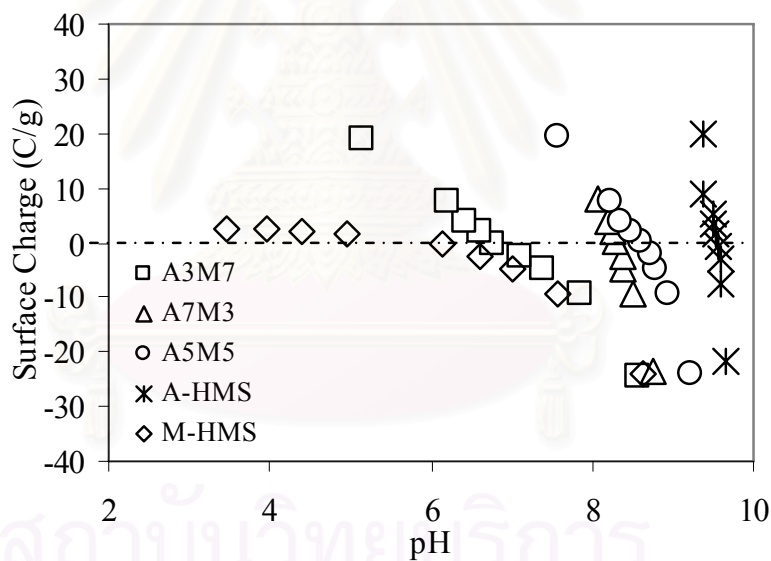

Figure 4.6 Surface charges of A-HMS, M-HMS, A3M7, A5M5, and A7M3 as a function of pH

Figure 4.5-4.6 showed the surface charge density of applied adsorbents as function of pH. The pH value that gives zero surface charge is defined as the zero point of charge (pH$_{ZPC}$). pH$_{ZPC}$ of all adsorbents was summarized in Table 4.2.

At this pH value, the positive charge of cationic surface groups and the negative charge of anionic surface groups are balanced. As shown in Figure 4.5-4.6, the surface charge density decrease as the pH increases from acidic region to neutral

pH. The silanol groups on the surface of HMSs gain or lose protons, resulting in surface charge variation at different pH as shown in the following equation. At low pH, surface sites of HMSs are protonated and the surfaces become positively charged; whereas at a high pH, the surface hydroxides lose their protons, and the surface becomes negatively charged.
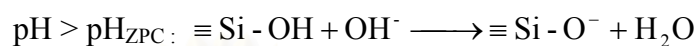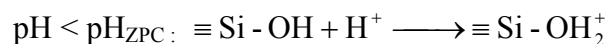
$$pH < pH_{ZPC :} \quad \equiv Si\text{-}OH + H^+ \longrightarrow \equiv Si\text{-}OH_2^+$$

$$pH > pH_{ZPC :} \quad \equiv Si\text{-}OH + OH^- \longrightarrow \equiv Si\text{-}O^- + H_2O$$

Table 4.2 pH_{ZPC} of PAC, HMS, SF-HMS, BF-HMS, NaY, HY zeolite and activated alumina

Adsorbents	pH_{ZPC}
PAC	9.5
HMS	5.5
A-HMS	9.5
M-HMS	6.2
A3M7	6.7
A5M5	8.6
A7M3	8.3
NaY zeolite	7.8
HY zeolite	4.5
Activated alumina	7.3

The amino-functional groups presented on HMS gave a higher pH_{ZPC} than pristine HMS. The amino groups are protonated and become positive charges on surface. Furthermore, surface charge of M-HMS did not change significantly at pH in range of 4-6.

4.2 Adsorption Kinetic

The adsorption kinetic for DCAA adsorption was performed by varying contact time from 0 to 72 h under batch condition at DCAA concentration of 100 μg/l and amount of adsorbent of 2 g/l. The pH of solution was fixed at pH 7 by phosphate buffer. Samples were shaken in shaking water bath at 25°C, 150 rpm until equilibrium. The results were shown in Figure 4.7.

The adsorption of DCAA on PAC can reach equilibrium faster than others. The adsorption rate of DCAA on PAC increases dramatically in first 10 minutes and reached equilibrium stage at about 6 h. For HMS, functionalized HMSs, activated alumina, NaY and HY zeolite, the adsorption rates of DCAA significantly increases in the range of 1-6 h and reached equilibrium stage at around 24 h. PAC has faster adsorption rate comparing with synthesized HMSs, zeolite and alumina which might be caused by surface functional group complexity and its large surface area.

To analyze the adsorption rate of DCAA onto PAC, HMS, functionalized HMSs, Activated alumina, NaY and HY zeolite, the pseudo-first-order equation of Lagergren and the pseudo-second-order rate were evaluated base on the experimental data. The pseudo-first-order and pseudo-second-order kinetic model are expressed as Eq.4.4 and Eq.4.5.

$$\ln(q_e - q_t) = \ln q_e - k_1 t \qquad\qquad 4.4$$

$$\frac{t}{q_t} = \frac{1}{2k_2 q_e^2} + \frac{t}{q_e} \qquad\qquad 4.5$$

Where k_1 =   Lagergren rate constant (h^{-1})

     k_2 =   Pseudo-second-order rate constant ($g\ mg^{-1}\ h^{-1}$)

     q_e =   Amounts of DCAA sorbed at equilibrium (h)

     q_t =   Amounts of DCAA sorbed at time t (h)

The experimental data were plotted $\ln(q_e - q_t)$ versus time for first-order rate and plotted t/q_t versus time for second-order rate. The kinetic constants of adsorbents were calculated and listed in Table 4.3.

It was found that the pseudo-second-order model can be fitted for adsorption of DCAA onto every adsorbents indicated by the correlation coefficients comparing with pseudo-first-order model. It means the pseudo-second-order rate models could be

described adsorption kinetics for DCAA adsorption, based on the assumption that the adsorption step may involve chemisorption. Moreover, the experimental q_e values and the calculated q_e obtained from the linear plot in Eq. 4.5 were compared as shown in Table 4.3. The results in Table 4.3 exhibit very good consistency between that calculated q_e and experimental q_e.

Table 4.3 Kinetics values calculated for DCAA adsorption onto PAC, HMS, functionalized HMSs, activated alumina, NaY and HY zeolite

Adsorbent	Pseudo First-order		Pseudo Second-order				
	R^2	k_1	R^2	k_2	Calculated	Experimental	h
		(h^{-1})		$(g/\mu g\ h)$	$q_e\ (\mu g/g)$	$q_e\ (\mu g/g)$	$(\mu g/g\ h)$
PAC	0.721	1.997	1.000	0.094	38.760	38.605	141.220
HMS	0.723	0.159	0.986	0.073	12.438	12.141	11.293
A-HMS	0.874	1.649	1.000	0.523	5.924	5.801	18.354
M-HMS	0.982	0.596	0.996	0.210	8.418	7.692	14.881
A3M7	0.657	0.102	0.991	0.332	10.741	10.357	38.303
A5M5	0.674	0.095	0.995	0.612	6.423	7.139	25.248
A7M3	0.454	0.180	0.965	0.133	11.682	8.415	18.150
NaY	0.941	0.286	0.994	0.154	10.406	10.179	16.676
HY	0.931	0.313	0.997	0.254	11.655	11.290	34.503
Alumina	0.612	0.115	0.994	0.152	10.299	10.095	16.123

In addition, the initial adsorption rate can also be obtained from this model from Eq.4.6 showed in Table 4.3.

$$h = k_2 q_e^2 \qquad\qquad 4.6$$

Where h is the initial adsorption rate ($\mu g/g\ h$). From calculations, it showed that PAC had the highest initial adsorption rate and much more than others. The calculated data clearly agree with experimental data observed in Figure 4.7 that initial time, concentration of DCAA adsorbed onto PAC rapidly decrease, and then slowly decrease until equilibrium stage at 6 h.
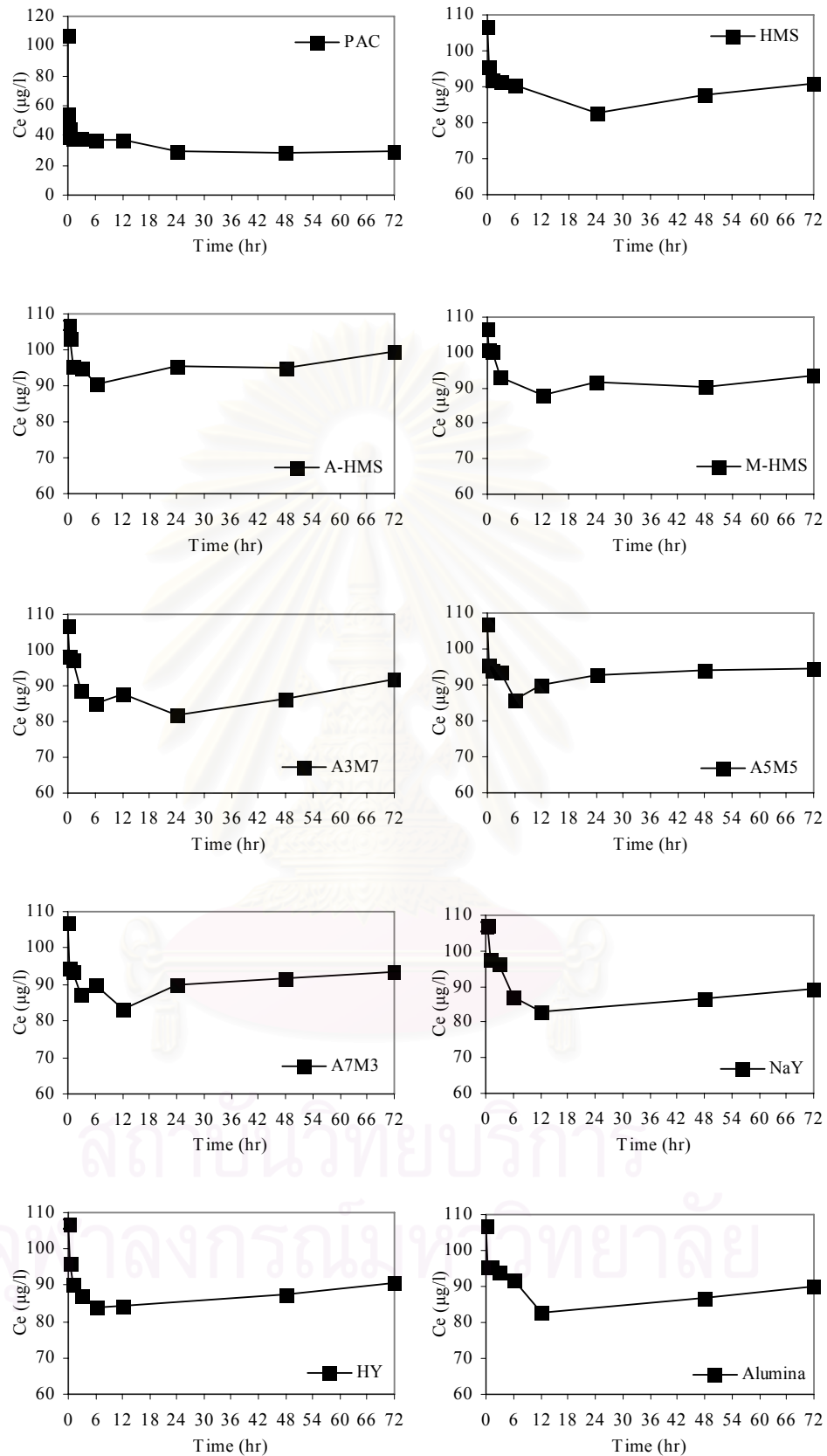
Figure 4.7 Adsorption kinetic of PAC, HMS, functionalized HMSs, Activated Alumina, NaY and HY zeolite

4.3 Adsorption Isotherm

In this study, adsorption mechanisms of DCAA from aqueous solution onto synthesized HMSs, Zeolite and alumina were investigated. Their adsorption capacities were compared with PAC. Physical characteristics of these materials were investigated and their effects to adsorption mechanisms were discussed. We employed the information from adsorption isotherm together with a theoretical evaluation of the surface properties of adsorbents and adsorbate to elucidate adsorption capacities and mechanisms of synthesized HMSs, Zeolite, alumina and PAC. Moreover, the experimental results were fitted to Langmuir and Freundlich Equations.

4.3.1 Effect of Surface Functional Groups

The adsorption experiments were conducted at pH 6.0-7.5. Therefore, DCAA which has pKa at 1.30 can dissociate to dichloroacetate ion almost 100 percent. Negative charge of DCAA was expected to enhance adsorption capacity due to electrostatic attraction with positively charged adsorbent. From obtained surface charge of adsorbents, HMS and M-HMS exhibit nearly zero charge in the range of pH of 4-6. At this range the electrostatic attraction between their surfaces and negative charge of DCAA can be neglected. In addition, HMSs functionalized by amino-functional groups including A-HMS, A5M5 and A7M3 exhibit strongly positive charge at that range of pH except A3M7 which had almost neutral (weak positive charge). Figure 4.8-4.9 shows adsorption isotherms of HMS, M-HMS, A-HMS, A3M7, A5M5 and A7M3.

It was expected that A-HMS which exhibits positive charge on surface could enhance adsorption capacity for DCAA by electrostatic attraction by negative charge of DCAA and positive charged surface. However, It was found that at low level concentration (0-400 ppb), effect of electrostatic attraction could not enhance adsorption capacity significantly. On contrary, Punyapalakul P. and Takizawa S. (2004) was reported that significantly increasing of adsorption capacity for DCAA on synthesized HMSs was detected at high level concentration (0-100 ppm) due to more positively charged HMSs. Moreover, effect of surface functional groups complexity cannot be detected at low level concentration. In addition, it might be indicated that

at low concentration, hydrophilicity of adsorbent plays more important role than electrostatic attraction force.
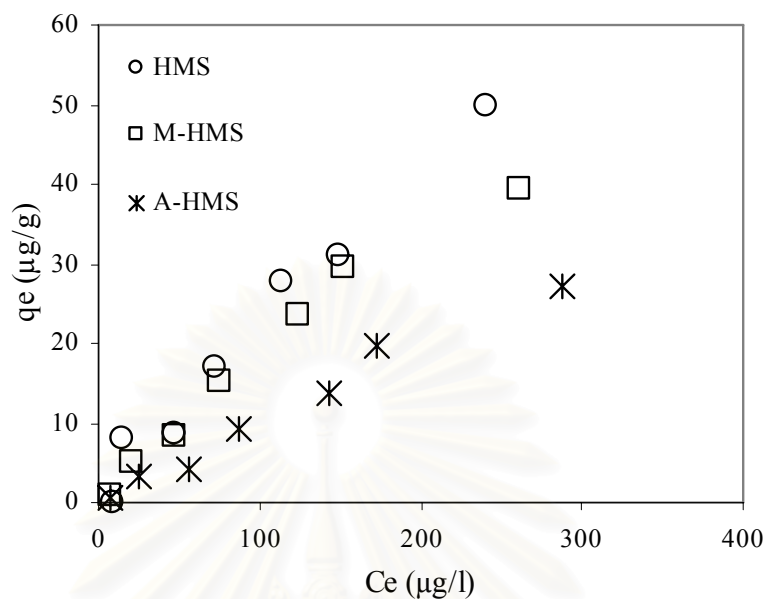

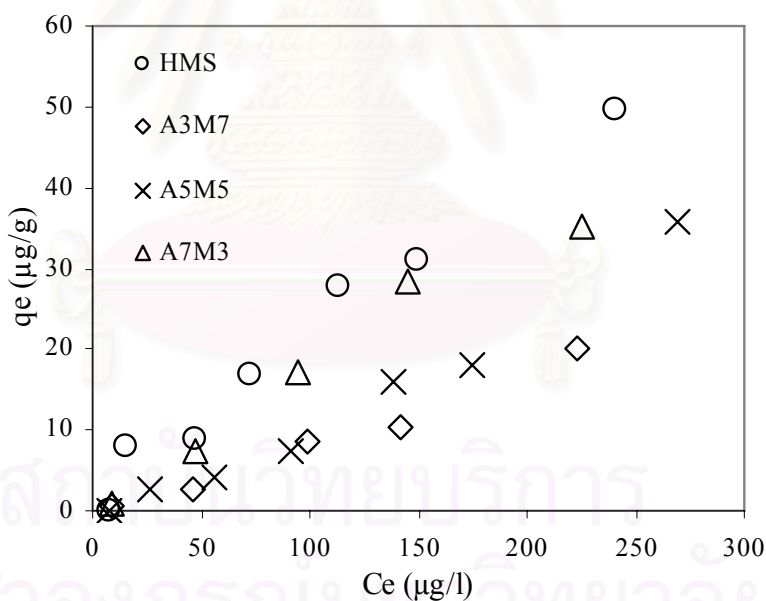**Figure 4.8** Adsorption capacities of HMS, M-HMS and A-HMS

Figure 4.9 Adsorption capacities of HMS, A3M7, A5M5 and A7M3

Moreover, M-HMS, higher hydrophobicity, exhibited comparable adsorption capacity as HMS. Functional groups on M-HMS surface still have silanol groups confirmed by FT-IR spectra. It implies that remained silanol groups on surface of M-HMS still can affect to adsorption of DCAA at low concentration. However, at concentration higher 300 ppb, DCAA had lower adsorption capacity than HMS

significantly, which can be caused by limitation of remained silanol group on M-HMS surface. Furthermore, despite surface charge of M-HMS is almost neutral as same as HMS at this pH, adsorption capacity of A-HMS could be detected. Hence, it can be concluded that adsorption capacity for DCAA adsorption at low concentration is not dependent on surface charge of adsorbents.

For BF-HMSs, the presence of mercapto-functional groups combined with amino-functional groups at the ratio of 3:7 (A7M3) dramatically exhibits higher adsorption capacity than A-HMS. This phenomenon is similar to DCAA adsorption at high concentration (Punyapalakul P. and Takizawa S., 2004). Moreover, DCAA adsorption capacity of A5M5 was almost same as A-HMS, although a little bit higher adsorption capacity of A5M5 at concentration higher than 300 ppb was detected. For A3M7, adsorption capacity was almost equal to A-HMS. From obtained results, it can be concluded that ratio of amino to mercapto functional groups is consistent with adsorption capacity for DCAA adsorption. Adsorption capacity of DCAA can be enhanced by increasing of the ratio of amino to mercapto functional groups.

From data on specific surface area of adsorbents, M-HMS had larger specific surface area than HMS. It was expected that M-HMS should have higher DCAA adsorption capacity than HMS. But the result in Figure 4.8 showed different information. Correspondingly, A3M7 also had larger specific surface area than A5M5 and A7M3. It was expected higher adsorption capacity than A5M5 and A7M3. However, A7M3 which had the lowest BET surface area gave the highest adsorption capacity. Hence, it can be addressed that the adsorption capacity of DCAA adsorption was not significantly dependent on specific surface area of adsorbents but extensively dependent on surface functional groups and hydrophilicity.

According to molecular size of DCAA (0.69 nm and 0.46 nm in width and length) (Punyapalakul and Takizawa, 2004) is smaller than pore size of all adsorbents, therefore, molecular size should not affect to accessibility of DCAA into mesopore of adsorbents. However, micropore of PAC might enhance adsorption capacity by increasing molecular sieve characteristic combining with electrostatic force and surface complexity.

The parameters and correlation coefficients of Langmuir and Fruendlich isotherm model were calculated by using experimental data through linear regression were listed in Table 4.4. It can be seen that correlation coefficients of Langmuir isotherm and Freundlich isotherm were not different significantly. However, obtained

data were plotted by non-linear estimation of STATISTICA version 6.0. It was found that obtained data had no relationship with Langmuir isotherm. On the other hand, Freundlich isotherm can be fitted to the data with very high correlation coefficients.

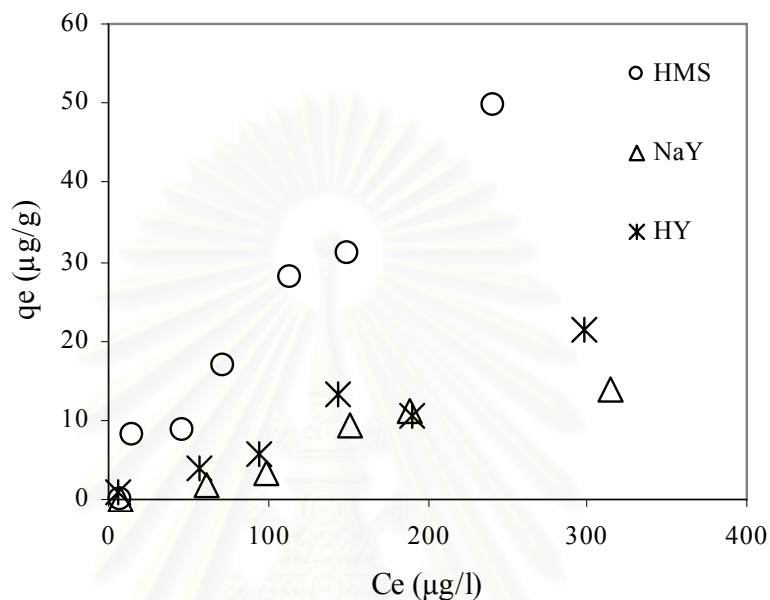### 4.3.2 Effect of Crystalline Structure

Figure 4.10 Adsorption capacities of HMS, NaY, and HY zeolite

In addition, effects of crystalline structure of HMS, NaY and HY zeolites were studied. Adsorption isotherms of HMS, NaY and HY were shown in Figure 4.10. This result showed that HMS had adsorption capacity higher than NaY and HY zeolite. It might be caused by small amounts of silanol group on NaY and HY zeolite comparing with HMS. According to aluminum atom inside silicate structure of Faujasite Y, it can exhibit a negative charge on oxygen atoms and might be balanced by counter ions (such as Na^+, H^+ and K^+) as shown in Figure 4.11. Hence, it can be suggested that crystalline structure might affect to adsorption capacity of DCAA.
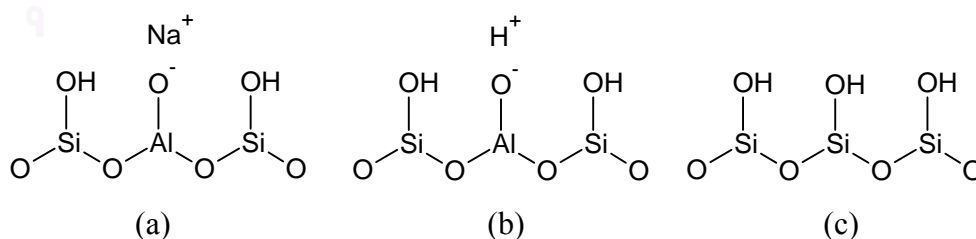

Figure 4.11 Crystalline structures of (a) NaY zeolite, (b) HY zeolite and (c) HMS

From Figure 4.10, HY zeolite showed a little bit higher adsorption capacity than NaY zeolite although crystalline structures are same. It is noticeable that counter ions on surface of zeolite can affect to DCAA adsorption capacity. It could be suggested that as protons of HY zeolite having positive charge similar to sodium ions on NaY zeolite, but size of proton is much smaller than sodium ion. It means that proton on HY zeolite has higher charge density than sodium ions of NaY zeolite, causing higher adsorption capacity.
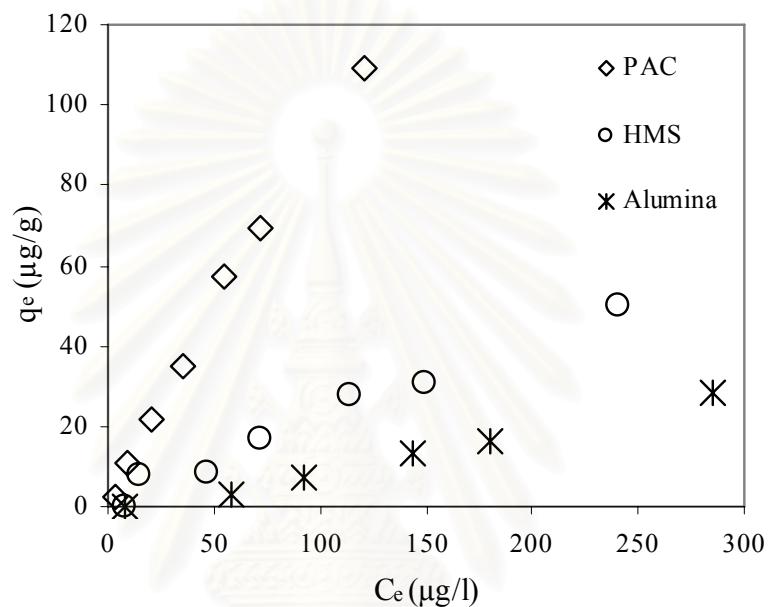

Figure 4.12 Adsorption capacities of PAC, HMS, and activated alumina

From Figure 4.12, PAC showed much higher adsorption capacity than HMS and activated alumina. It might be caused by surface complexity of PAC inducing many interaction forces involved such as electrostatic force, van der Waals force and covalent bonding. Activated alumina showed lower adsorption capacity than HMS. It is suggested that hydrogen bonding between alumina and DCAA is weaker than hydrogen bonding between silanol groups of HMS and DCAA.

Table 4.4 Parameters of Langmuir and Freundlich isotherm model for DCAA adsorption on PAC, HMS, functionalized HMS, Activated alumina, NaY and HY zeolite at pH 5, 7 and 9

Adsorbent	Langmuir			Freundlich		
pH	q_m	K_L	R^2	K_F	n	R^2
PAC						
5	322.581	0.0086	0.987	1.102	0.820	0.980
7	294.118	0.0040	0.996	0.991	1.000	0.994
9	7.788	0.0415	0.935	0.928	2.587	0.865
HMS						
5	250.000	0.0006	0.994	0.157	1.055	0.987
7	256.410	0.0010	0.986	0.904	1.420	0.886
9	212.766	0.0003	0.987	0.024	0.820	0.950
A-HMS						
5	322.581	0.0004	0.991	0.158	1.104	0.983
7	312.500	0.0003	0.980	0.091	0.980	0.976
9	285.714	0.0001	0.993	0.024	0.878	0.922
M-HMS						
5	243.902	0.0013	0.997	0.397	1.152	0.988
7	238.095	0.0011	0.994	0.175	0.949	0.994
9	185.185	0.0001	0.984	0.004	0.652	0.976
A3M7						
5	303.030	0.0010	0.972	0.424	1.282	0.962
7	294.118	0.0002	0.998	0.056	0.933	0.990
9	285.714	0.0001	0.991	0.003	0.673	0.955
A5M5						
5	344.828	0.0003	0.999	0.101	0.984	0.991
7	357.143	0.0003	0.960	0.045	0.855	0.970
9	294.118	0.0001	0.981	0.010	0.731	0.996
A7M3						
5	227.273	0.0005	0.999	0.092	0.932	0.997
7	232.558	0.0009	0.965	0.093	0.887	0.994
9	196.078	0.0003	0.993	0.052	0.973	0.934
NaY						
5	17.123	0.0008	0.981	0.004	0.638	0.993
7	26.110	0.0038	0.983	0.001	0.585	0.980
9	16.863	0.0002	0.984	0.0003	0.491	0.995
HY						
5	23.753	0.0210	0.994	0.636	1.338	0.999
7	15.674	0.0086	0.991	0.159	1.200	0.966
9	13.459	0.0003	0.978	0.0003	0.497	0.999
Alumina						
5	24.155	0.0483	0.983	1.435	1.691	0.975
7	16.667	0.0006	0.969	0.003	0.602	0.990
9	15.314	0.0027	0.693	0.002	0.613	0.963

4.4 Adsorption Mechanisms

In order to determine adsorption mechanism of DCAA, the effect of pH and temperature on adsorption capacity of adsorbents were evaluated and discussed below;

4.4.1 Effect of pH

To reveal the importance of the electrostatic interaction between the positive charge of adsorbent and negative charge of DCAA, the effects of pH on the adsorption capacity of PAC, HMS, functionalized HMSs, activated alumina, NaY, and HY zeolite were investigated by varying pH of solution from 5-9 controlled by phosphate buffer.
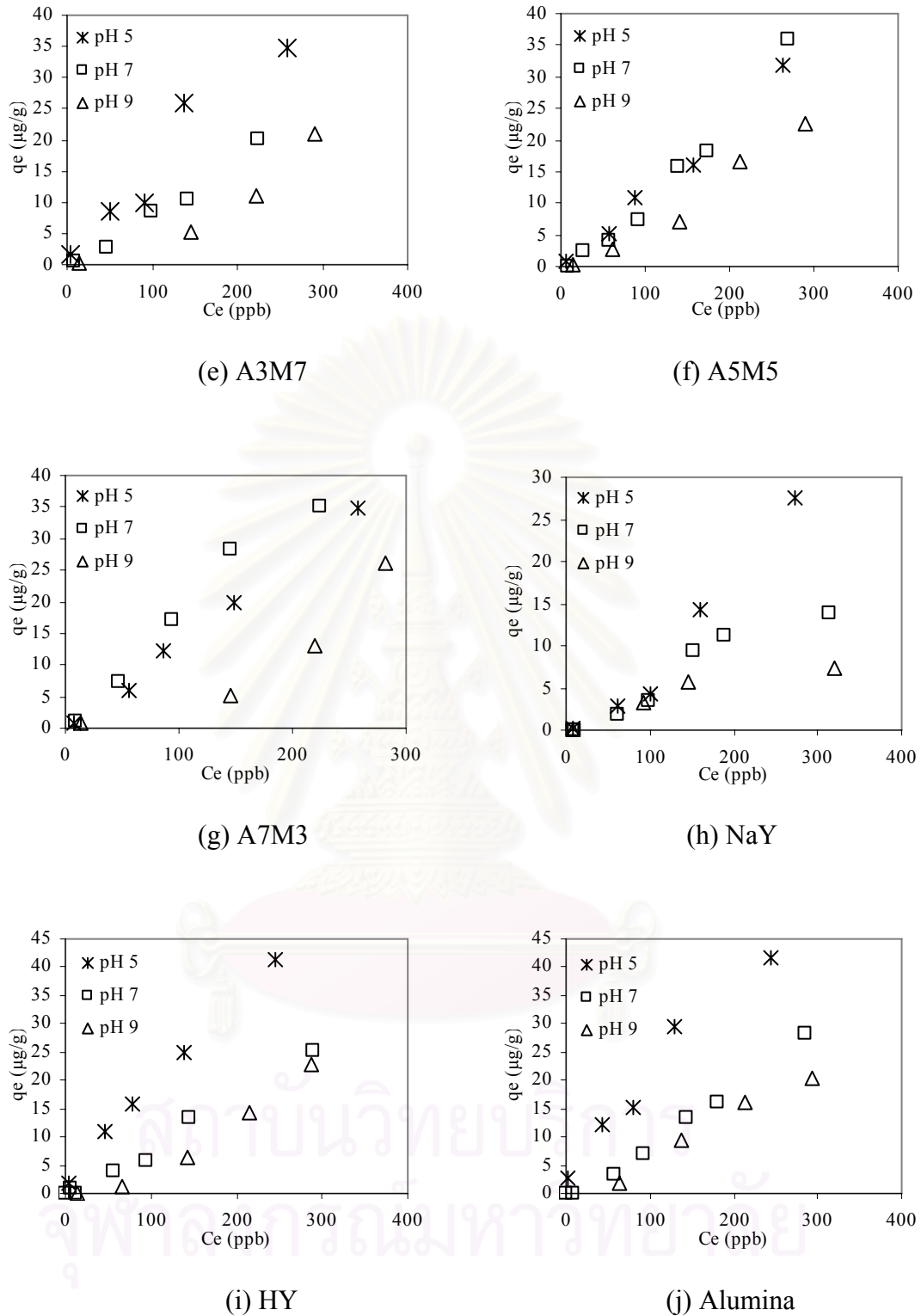

(a) PAC

(b) HMS

(c) A-HMS

(d) M-HMS

(e) A3M7   (f) A5M5

(g) A7M3   (h) NaY
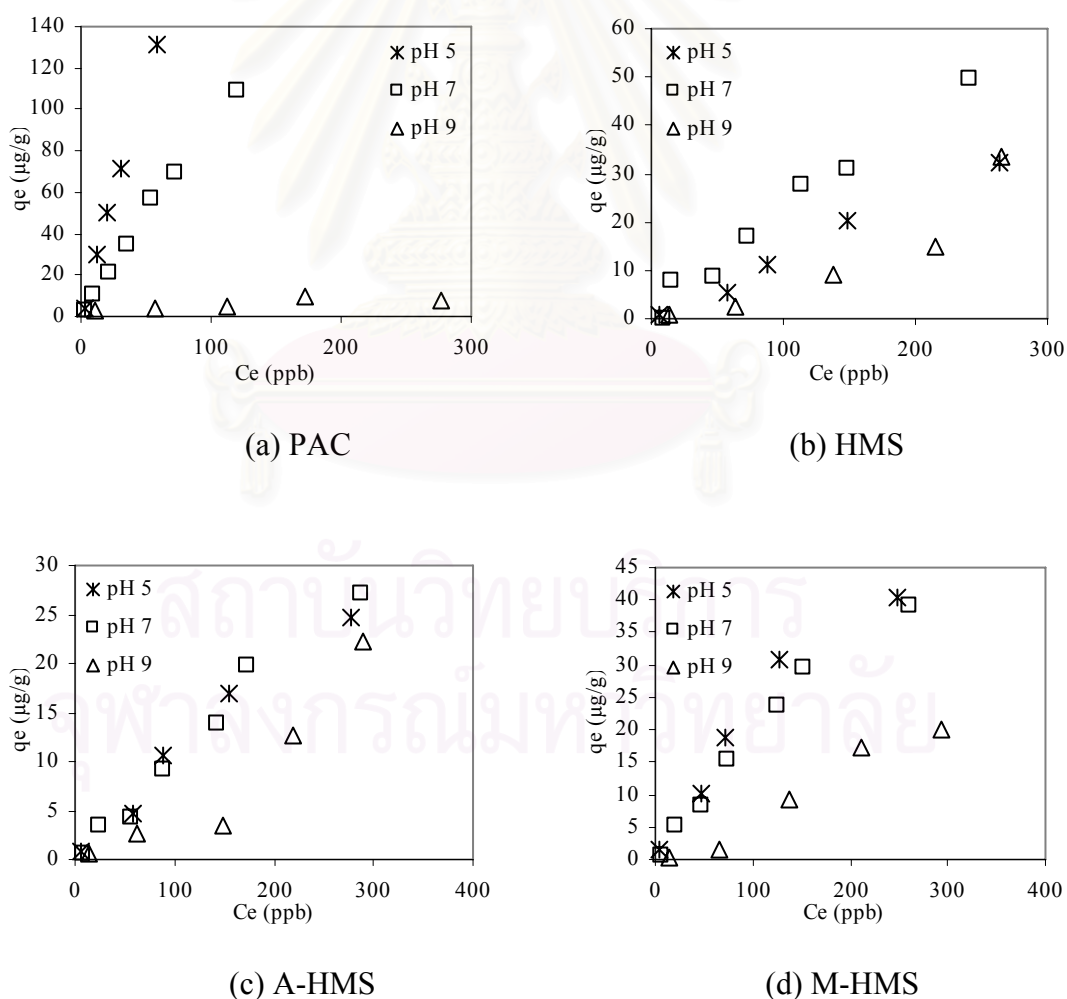
(i) HY   (j) Alumina

Figure 4.13 Adsorption capacities of (a) PAC, (b) HMS, (c) A-HMS, (d) M-HMS,
(e) A3M7, (f) A5M5, (g) A7M3, (h) NaY, (i) HY and (j) Alumina at different pH

Figure 4.13 (a) showed adsorption capacity of PAC at pH 5-9. At pH 5, surface of PAC had higher positive charge than pH 7 which can enhance adsorption capacity by electrostatic attraction. On contrary, PAC would be deprotonated and change to be negative charge at pH 9. Hence, repulsion force between negatively charged of PAC surface and negatively charged of DCAA can decrease DCAA adsorption capacity of PAC. From obtained data, it can be concluded that the adsorption capacity of DCAA on PAC was significantly affected by pH causing electrostatic interaction between PAC and DCAA.

As same as PAC, adsorption capacity DCAA on NaY, HY and activated alumina was affected by pH. As shown in Figure 4.13 (j), adsorption capacity of activated alumina was increased by decreasing of pH due to electrostatic interaction.

At pH higher than pH_{ZPC}, silanol groups of HMS will be loosed protons from surface, negatively charged on surface of silanol goups can be increased as shown in Figure 4.14. This mechanism causes repulsion force between negatively charged of DCAA and negatively charged of silanol groups. Hence adsorption capacity of HMS at pH 9 was lower than pH 7. However, at pH 5, adsorption capacity of HMS was decreased even neutral charge of HMS surface did not change significantly from pH 4-6. It might be caused by electrostatic interaction between water and DCAA. Water can be protonated to be hydronium ion which exhibits stronger positive charge. Hence, interaction between DCAA and HMS surface might be interfered by stronger electrostatic interacting between hydronium ion and DCAA, especially at low pH and low level concentration.

Adsorption capacities of functionalized HMSs were not affected by pH except A3M7 and M-HMS as shown in Figure 4.13 (c) (d) (e) (f) and (g). At pH 5 and 7, surface charge of A-HMS, M-HMS, A7M3 and A5M5 did not change significantly. Therefore, adsorption capacities of these adsorbents were not affected by decreasing pH. However, DCAA adsorption capacity of A3M7 was affected by decreasing of pH from 7 to 5, consistent with increase of positive charge of A3M7 surface. Moreover, at pH 9, surface charge of all functionalized HMSs was decreased rapidly that caused clearly decreasing of adsorption capacities.
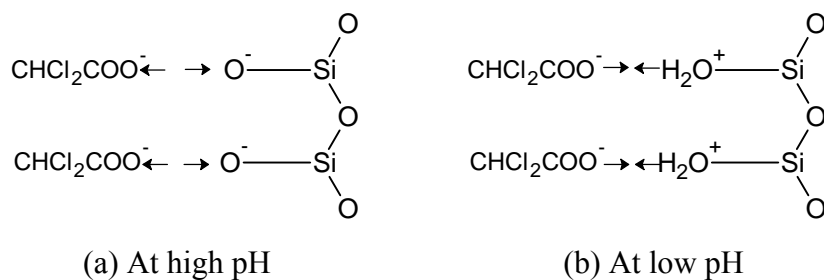
(a) At high pH   (b) At low pH

Figure 4.14 Schematic representation of adsorption mechanism of DCAA and silanol groups at (a) high and (b) low pH

4.4.2 Effect of Temperature

         To study effect of temperature on DCAA adsorption capacity of applied adsorbents, temperature of adsorption experiments was varied from $25 - 60°C$. PAC, HMS, activated alumina and NaY zeolite were selected as model adsorbents in this study.

(a) PAC   (b) HMS
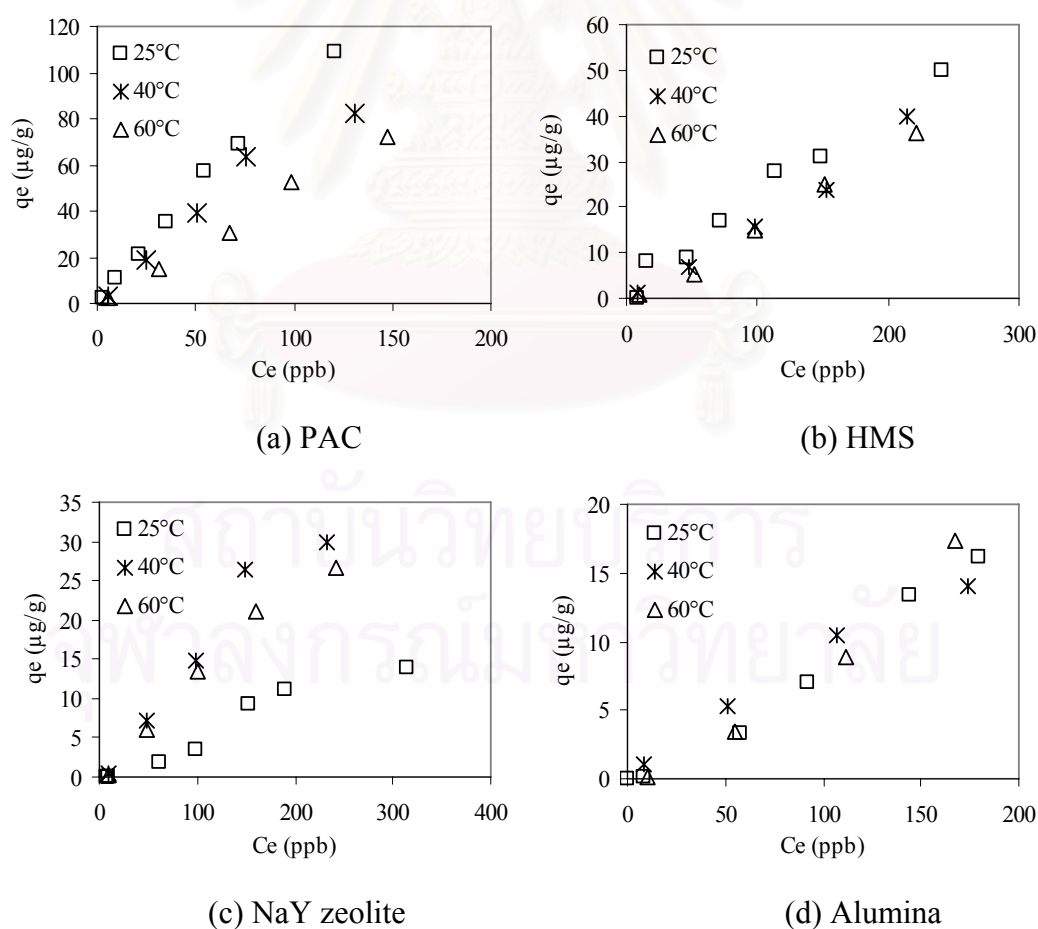
(c) NaY zeolite   (d) Alumina

Figure 4.15 Adsorption capacities of (a) PAC, (b) HMS, (c) NaY, and (d) activated alumina at different temperature

Figure 4.15 showed the adsorption capacities of PAC, HMS, NaY zeolite and activated alumina at different temperature. It is clear that the DCAA adsorption capacity of PAC decreased with increasing temperature. It might be assumed that DCAA adsorption on PAC was physical adsorption. On contrary, DCAA adsorption capacity of NaY zeolite increased with increase of temperature, suggesting that it might be involved chemical adsorption. However, limitation of increasing adsorption capacity by raising temperature was found. For HMS and activated alumina, the adsorption capacity for DCAA adsorption was not affected by temperature significantly.

CHAPTER V
CONCLUSIONS AND RECOMMENDATIONS

The ultimate goal of this study was to determine DCAA adsorption capacities of synthesized HMSs, zeolite and alumina in aqueous solutio. Their adsorption capacities were compared with PAC. Physico-chemical characteristics of these materials were investigated and the effects of pH and temperature on adsorption mechanisms were discussed also. The adsorption experiments were performed under batch condition at low DCAA concentration of 10-300 ppb.

This investigation presented that the XRD patterns of functionalized HMSs exhibited very broad peak, indicating that the mesostructure of functionalized HMSs was less order. The specific surface areas of functionalized HMSs were decreased due to increasing of amino functional group. PAC has the small average pore size and HMS and functionalized HMSs have average pore sizes in the range of 2-50 nm. In addition, presence of organo-functional groups on HMS affects to the average pore size, especially, presence of amino-functional groups might deform hexagonal mesostructure which might cause increasing of average pore size. The FT-IR spectra of HMS and functionalized HMSs exhibit O-H stretching band at wavenumber of 3400-3500 cm^{-1}, indicating that they still have silanol groups on surface, particularly in HMS. C-H stretching and C-H bending bands of CH_2-methylene group appeared in functionalized HMSs, in spite of disappearance in HMS. Moreover, two N-H stretching bands of A-HMS indicate the presence of NH_2 but mercapto-functional groups (SH) in M-HMS and BF-HMSs could not be identified. However, they could be investigated by elemental analysis which confirmed that amino and mercapto functional groups presented on the surface of functionalized HMSs. pH_{ZPC} of PAC, HMS, activated alumina, NaY and HY zeolite was found to be 9.5, 5.5, 7.3, 7.8, and 4.5, respectively. And pH_{ZPC} of functionalized HMSs, A-HMS, M-HMS, A3M7, A5M5, and A7M3 was 9.5, 6.2, 6.7, 8.6, and 8.3, respectively. The presence of amino-functional groups on HMS gave a higher pH_{ZPC} than HMS, despite that M-HMS did not change significantly at pH in range of 4-6.

Adsorption kinetic follows the pseudo-second-order model for DCAA adsorption on all adsorbents, indicating that the adsorption step may involve chemisorption. The calculated q_e values agree well with the experimental q_e values.

DCAA adsorption capacity at low concentration did not affected by physical characteristics (e.g. surface area, pore size). Hydrophilicity of adsorbent plays more important role than electrostatic attraction force and surface area. Crystalline structure might affect to DCAA adsorption capacity. Correlation coefficients of Langmuir and Freundlich isotherm calculated by linear regression were not different significantly. However, it had no relationship with Langmuir isotherm from non-linear estimation.

DCAA adsorption capacity was significantly affected by pH depending on pH_{ZPC} of adsorbents. It can be concluded that not only hydrophilicity affected but also electrostatic attraction force.

Adsorption of DCAA on PAC was decreased by increasing of temperature, suggesting that adsorption of DCAA on PAC might involve physical adsorption. The opposite effect is observed for DCAA adsorption on NaY zeolite. It is suggested that DCAA adsorbed on NaY zeolite through chemisorption. DCAA adsorption capacity was not affected by temperature significantly for HMS and activated alumina.

Although the adsorption capacity of PAC is higher than HMSs and zeolites, but adsorption capacity of HAAs might be interrupted by co-existing compounds in water, for example natural organic matter, electrolytes, etc. Pore blockage and active site competition between target pollutant (HAAs) and co-existing compounds can be occurred due to high complexity of surface functional groups on PAC surface. On the other hand, pristine HMS which has higher adsorption capacity than functionalized HMSs and zeolites was expected higher selectivity since its uniform surface structure and functional groups. Thus, adsorption by combination of HMS and PAC in series might enhance overall pollutants removal efficiency. HAAs might be removed by HMS without site competition. Then, others coexisting-pollutants can be removed continuously by PAC. Adsorption capacities and regeneration periods for target pollutant of both HMS and PAC are suggested to be higher and longer respectively. Synthesis cost of HMS is still high (approximately 20 Baht/g) comparing with PAC. However, HMS is suggested to be regenerated easily by thermal regeneration without lost and decreasing of adsorption capacity. Hence, cost-benefit analysis for using HMS combining with PAC at the end-of-pipe of water supply system is still needed.

REFERENCES

Aprile C.; Abad A.; García H.; and Corma A. 2005. Synthesis and catalytic activity of periodic mesoporous materials incorporating gold nanoparticles. <u>Journal of Materials Chemistry</u> 15: 4408-4413.

Beck J.S.; Vartuli C.; Roth W.J.; Leonowicz M.E.; Kresge C.T.; Schmitt K.D.; Chu C.T-W.; Olson D.H.; Sheppard E.W.; McCullen S.B.; Higgins J.B.; and Schlenker J.L. 1992. A new Family of Mesoporous Molecular Sieves Prepared with Liquid Crystal Templates. <u>J. Am. Chem. Soc.</u> 114: 10834-10843.

Bjelopavlic M.; Newcombe G.; and Hayes R. 1999. Adsorption of NOM onto activated carbon: Effect of surface charge, ionic strength, and pore volume distribution. <u>Journal of Colloid and Interface Science</u> 210 (2): 271-280.

Bureau of Reclamation, Technical Service Center. 2003. <u>DBP: Haloacetic acids fact sheet</u>[Online]. Available from: http://www.usbr.gov/pmts/water/media/pdfs/DBP%_20HAAs.pdf[2006, November 1]

Crittenden J.C.; Trussell R.R.; Hand D.W.; Howe K.J.; and Tchobanoglous G. (n.d.). <u>Water treatment: principles and design.</u> 2nded. (n.p.): John Wiley & Sons, Inc.

Daniel C.H. (2003). <u>Quantitative chemical analysis sixth edition</u>. New York: W.H. Freeman and company.

Dojlido J.; Zbieć E.; and Ŝwietlik R. 1999. Formation of the haloacetic acids during ozonation and chlorination of water in Warsaw waterworks (Poland). <u>Water Research</u> 33 (14): 3111-3118.

Eren Z., and Acar F.N. 2007. Equilibrium and kinetic mechanism for Reactive Black 5 sorption onto high lime Soma fly ash. <u>Journal of Hazardous Materials</u> 143: 226-232.

Ghorai S., and Pant K.K. 2005. Equilibrium, kinetics and breakthrough studies for adsorption of fluoride on activated alumina. Separation and Purification Technology 42: 265-271.

Hudson S.; Magner E.; Cooney J.; and Hodnett B.K. 2005. Methodology for the Immobilization of Enzymes onto Mesoporous Materials. J. Phys. Chem. B 109: 19496-19506.

Korshin G.V., and Jenson M.D. 2001. Electrochemical reduction of haloacetic acids and exploration their removal by electrochemical treatment. Electrochimica Acta 47: 747-751.

Krasner S.W., and Wright J.M. 2005. The effect of boiling water on disinfection by-product exposure. Water Research 39: 855-864.

Langmuir D. (1997). Aqueous Environmental Geochemistry. New Jersey: Prentice Hall.

Lee B.H.; Kim Y.H.; Lee H.J.; and Yi J.H. 2001. Synthesis of functionalized porous silicas via templating method as heavy metal ion adsorbents: the introduction of surface hydrophilicity onto the surface of adsorbents. Microporous and Mesoporous Materials 50 (1): 77-90.

Lin T.F., and Wu J.K. 2001. Adsorption of arsenite and arsenate within activated alumina grains: Equilibrium and kinetics. Water Research 35 (8): 2049-2057.

Maria Chong A.S., and Zhao X.S. 2004. Design of large-pore mesoporous materials for immobilization of penicillin G acylase biocatalyst. Catalysis Today 93-95: 293-299.

Mercier L., and Pinnavaia T.J. 2000. Direct synthesis of hybrid organic-inorganic nanoporous silica by a neutral amine assembly route: structure-function control by stoichiometric incorporation of organosiloxane molecules. Chem Mater 12: 188-196.

Messina P.V., and Schulz P.C. 2006. Adsorption of reactive dyes on titania-silica mesoporous materials. Journal of Colloid and Interface Science 299: 305-320.

Newalkar B.L.; Choudary N.V.; Turaga U.T.; Vijayalakshmi R.P.; Kumar P.; Komarneni S.; and Bhat T.S.G. 2003. Adsorption of light hydrocarbons on HMS type mesoporous silica. Microporous and Mesoporous Materials 65: 267-276.

Punyapalakul P., and Takizawa S. 2004. Effect of Organic Grafting Modification of Hexagonal Mesoporous Silicate on Haloacetic Acid Removal. Environmental Engineering Forum 44: 247-256.

Rodriguez M.J.; Sérodes J.B.; and Levallois P. 2004. Behavior of trihalomethanes and haloacetic acids in a drinking water distribution system. Water Research 38: 4367-4382.

Rossman L.A.; Brown R.A.; Singer P.C.; and Nuckols J.R. 2001. DBP formation kinetics in a simulated distribution system. Water Research 35 (14): 3483-3489.

Rouquerol F.; Rouquerol J.; and Sing K. (1999). Adsorption by powders and porous solids (principles, methodology and applications). London: Academic Press.

Singh T.S., and Pant K.K. 2004. Equilibrium, kinetics and thermodynamic studies for adsorption of As (III) on activated alumina. Separation and Purification Technology 36: 139-147.

Stein A.; Melde B.J.; and Schroden R.C. 2000. Hybrid Inorganic-Organic Mesoporous Silicates - Nanoscopic Reactors Coming of Age. Advanced Materials 12: 1403-1419.

Tanev P.T., and Pinnavaia T.J. 1996. Mesoporous Silica Molecular Sieves Prepared by Ionic and Neutral Surfactant Templating: A Comparison of Physical Properties. Chem. Mater. 8: 2068-2079.

Tung H.H.; Unz R.F.; and Xie Y.F. 2006. HAA removal by GAC adsorption. Journal-American Water Works Association 98 (6): 107-112.

U.S. Environmental Protection Agency. (1999). EPA guidance Manual Alternative Disinfectants and Oxidants. Washington, D.C.: Office of Research and Development.

U.S. Environmental Protection Agency. (2001). Controlling Disinfection By-products and Microbial Contaminants in Drinking Water. Washington, D.C.: Office of Research and Development.

Volesky B. (n.d.). Sorption and Biosorption. (n.p.).

Weinberg H.S.; Pereira V.R.; Singer P.C.; and Savitz D.A. 2006. Considerations for improving the accuracy of exposure to disinfection by-products by ingestion in epidemiologic studies. Science of the Total Environment 354: 35-42.

Wobma P.; Pernitsky D.; Bellamy B.; Kjartanson K.; and Sears K. 2000. Biological filtration for ozone and chlorine DBP removal. Ozone-Science & Engineering 22 (4): 393-413.

Wu H.W., and Xie Y.F.F. 2005. Effect of EBCT and water temperature on HAA removal using BAC. Journal-American Water Works Association 97 (11): 94-101.

Xie Y.F.F., and Zhou H.J. 2002. Use of BAC for HAA removal-Part 2, column study. Journal-American Water Works Association 94 (5): 126-134.

Yiu H.H.P., and Wright P.A. 2005. Enzymes supported on ordered mesoporous solids: a special case of an inorganic-organic hybrid. Journal of Materials Chemistry 15: 3690-3700.

Yokoi T. 2004. Studies on the syntheses and applications of organic-functionalized mesoporous silica. Doctor's Thesis. Division of Materials Science and Engineering, Graduate School of Engineering, Yokohama National University.

Yoshitake H.; Koiso E.; Horie H.; and Yoshimaru H. 2005. Polyamine-functionalized mesoporous silicas: Preparation, structural analysis and oxyanion adsorption. Microporous and Mesoporous Materials 85: 183-194.

Zhou H.J., and Xie Y.F.F. 2002. Using BAC for HAA removal-Part 1: Batch study. Journal-American Water Works Association 94 (4): 194-200.
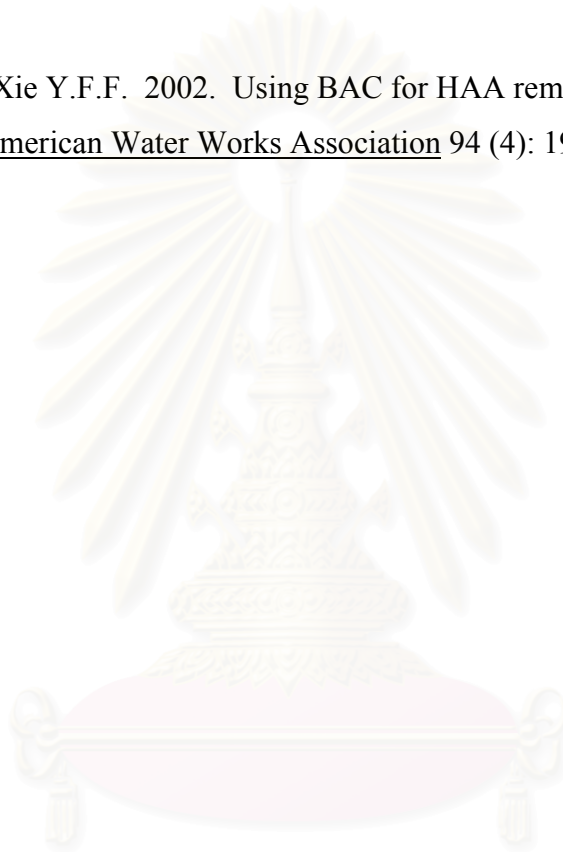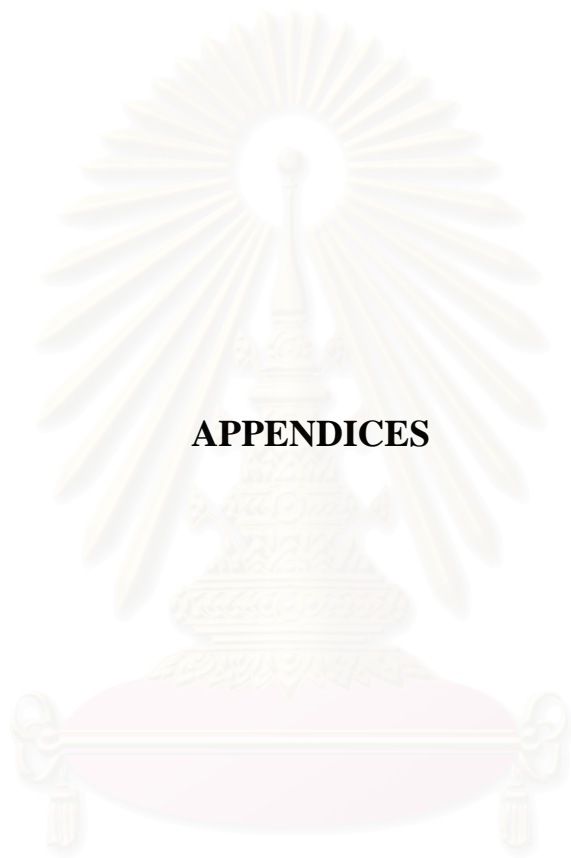
APPENDICES

APPENDIX A

Isotherm Linear Plot
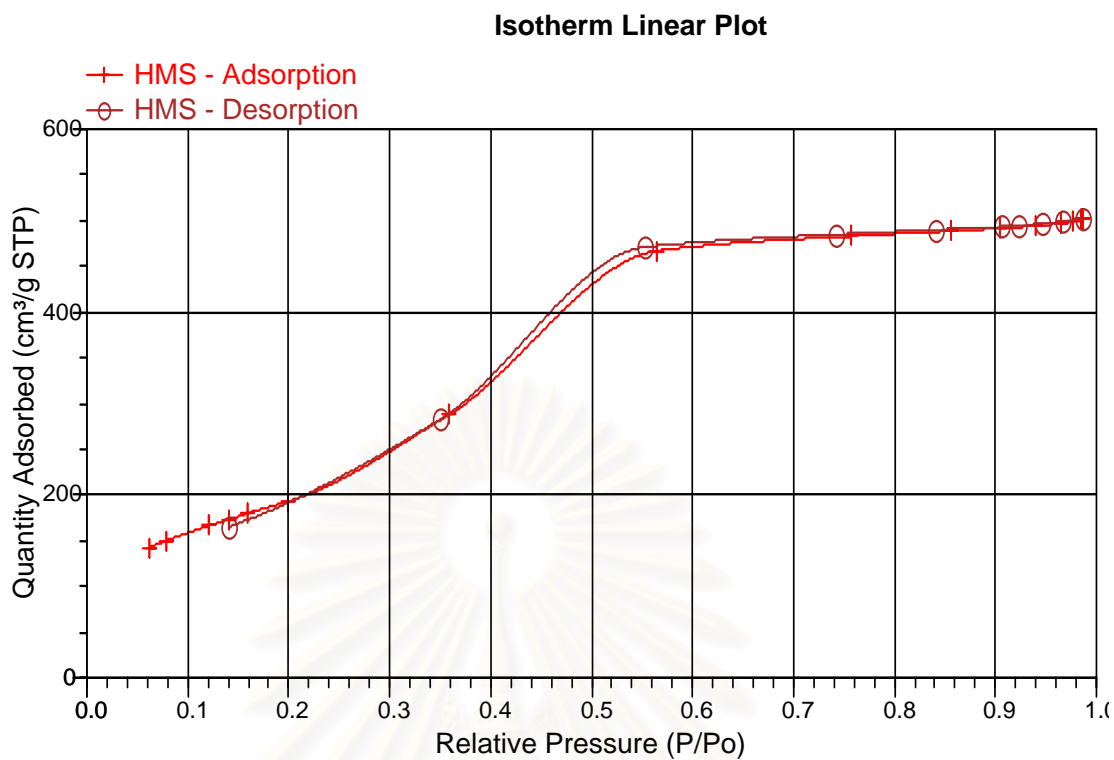
Figure A1 Nitrogen adsorption-desorption isotherm of HMS

Isotherm Linear Plot
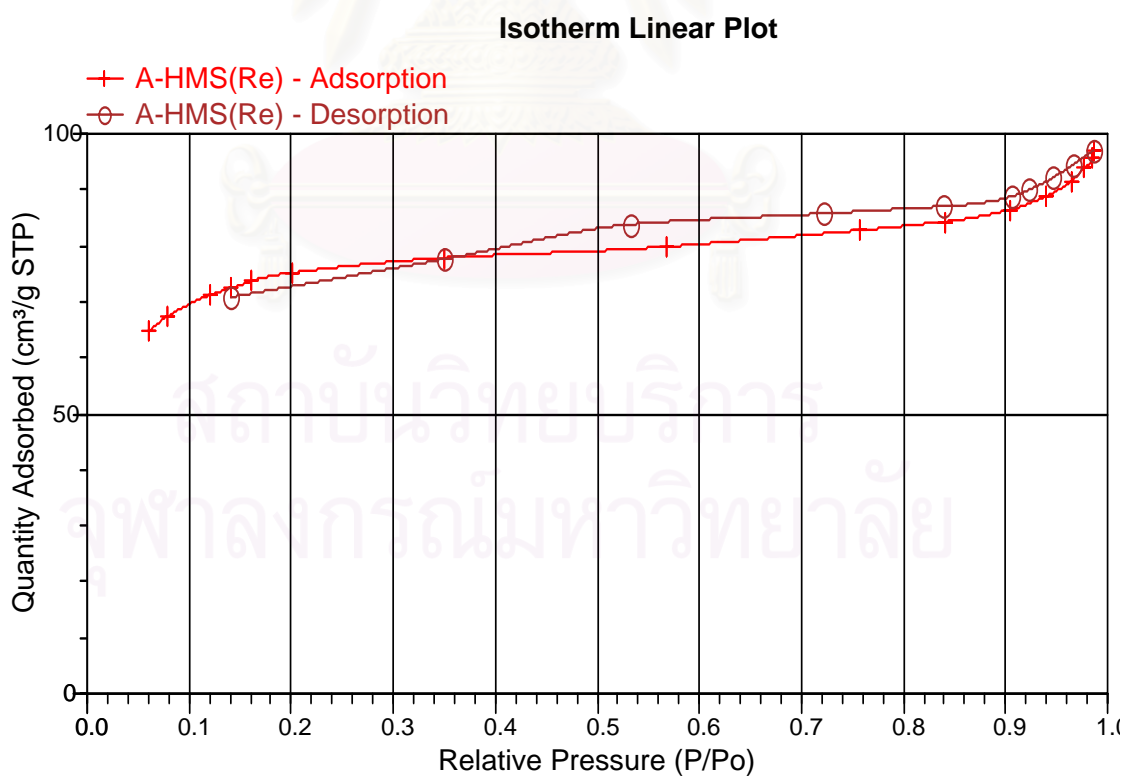
Figure A2 Nitrogen adsorption-desorption isotherm of A-HMS

Isotherm Linear Plot
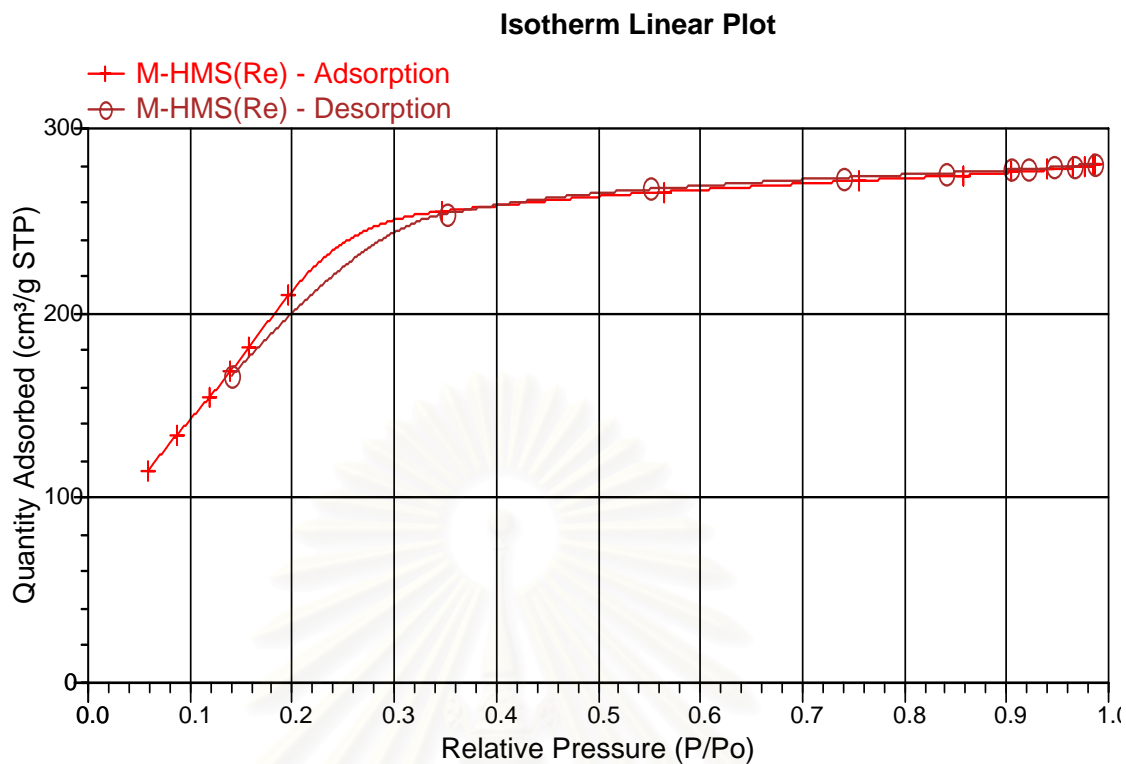
Figure A3 Nitrogen adsorption-desorption isotherm of M-HMS

Isotherm Linear Plot
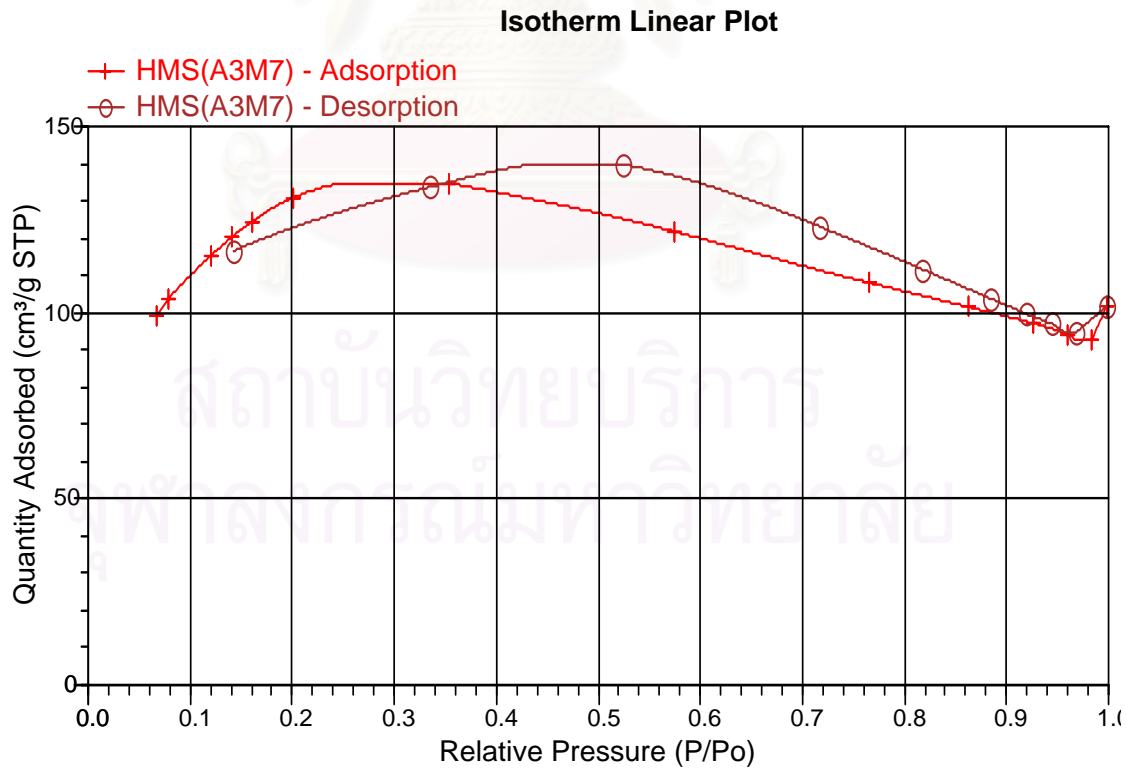
Figure A4 Nitrogen adsorption-desorption isotherm of A3M7

Isotherm Linear Plot
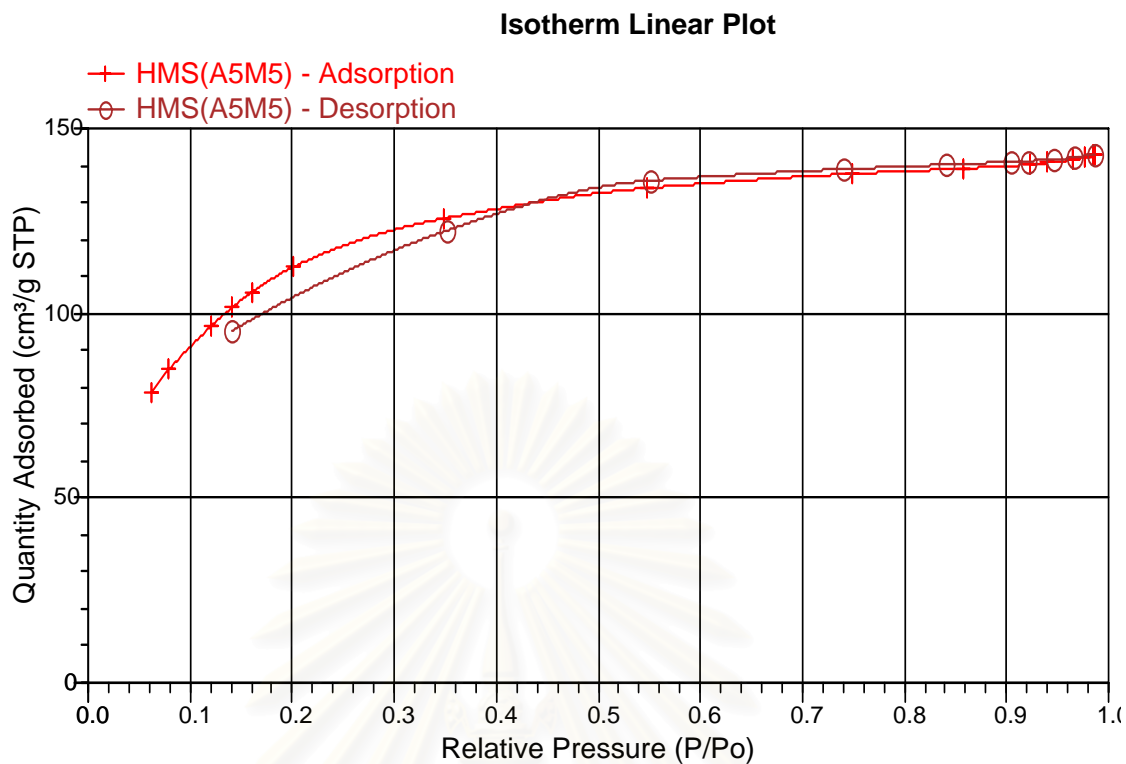
Figure A5 Nitrogen adsorption-desorption isotherm of A5M5

Isotherm Linear Plot
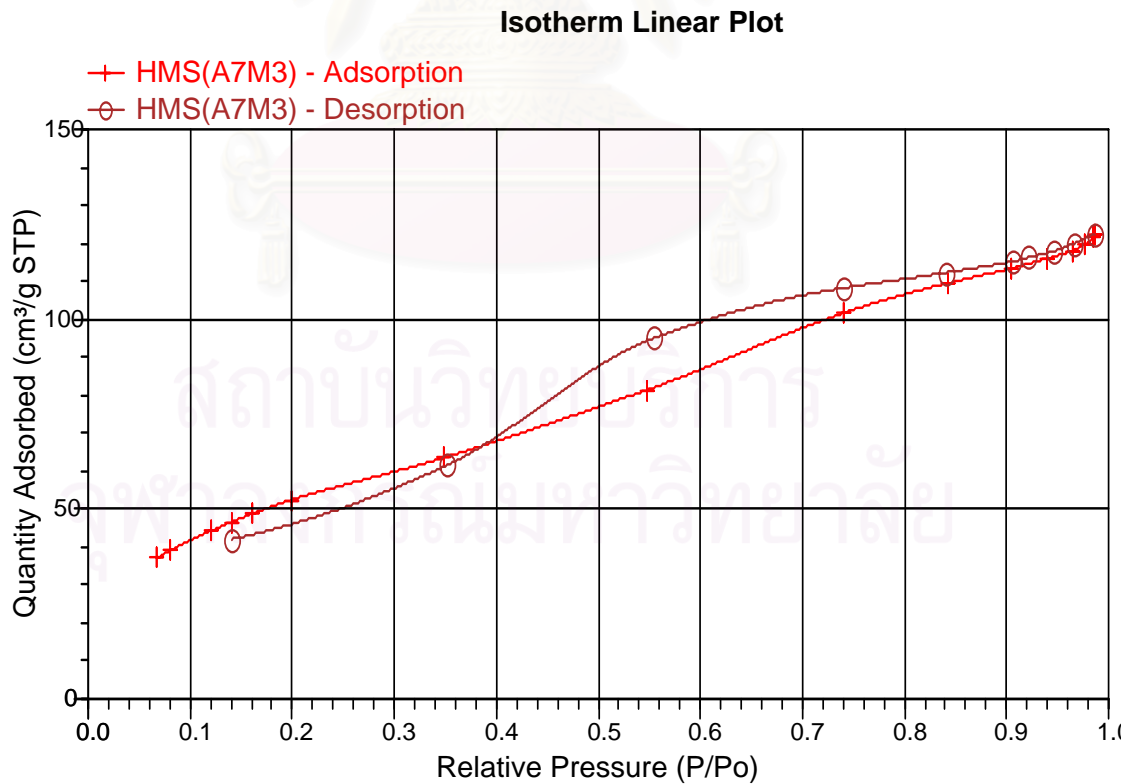
Figure A6 Nitrogen adsorption-desorption isotherm of A7M3

Isotherm Linear Plot
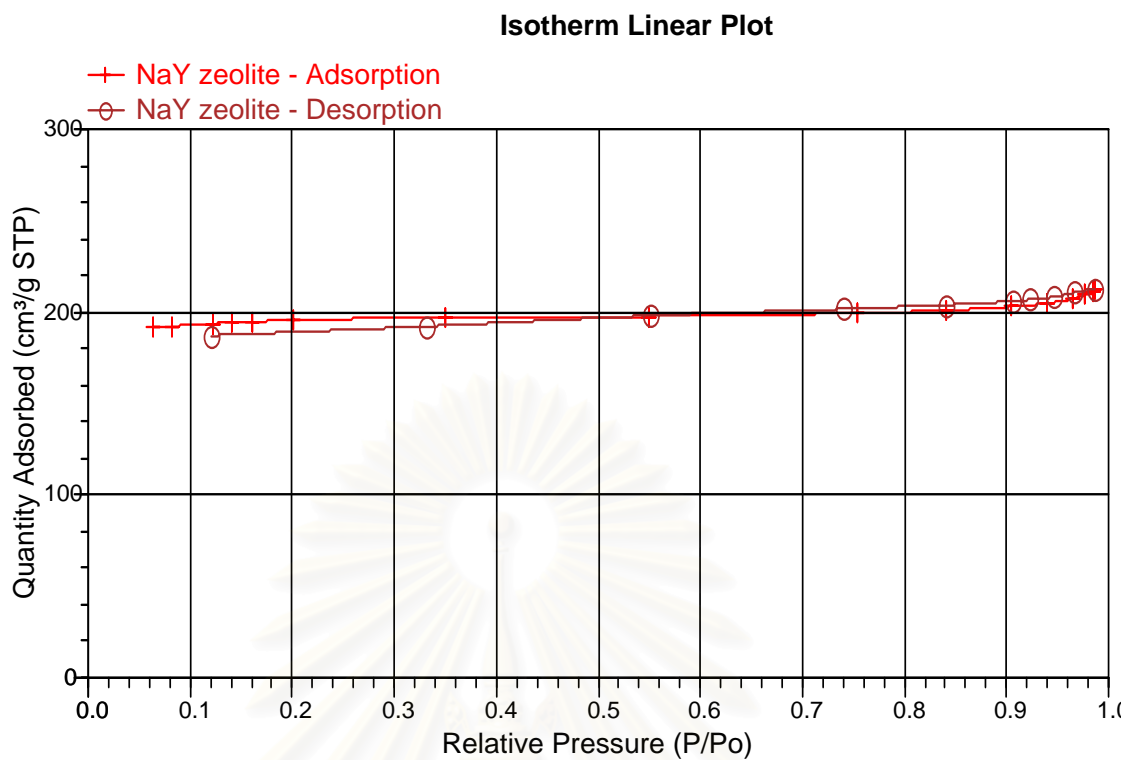
Figure A7 Nitrogen adsorption-desorption isotherm of NaY zeolite
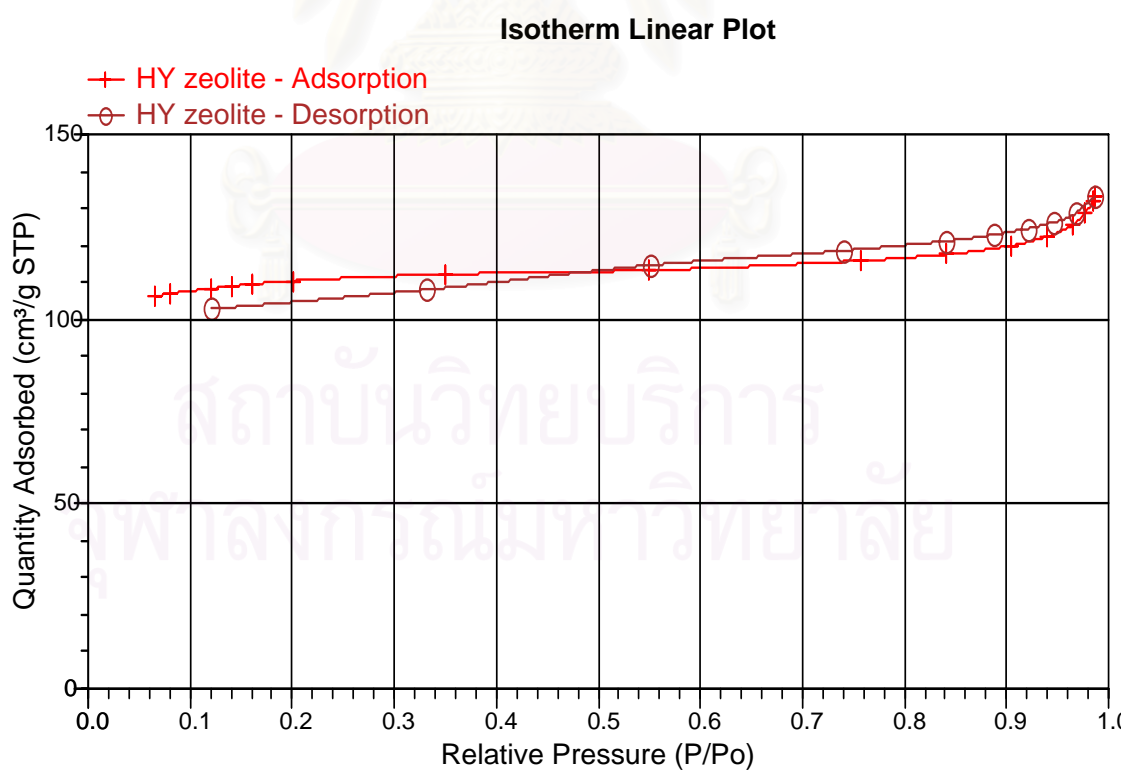
Isotherm Linear Plot

Figure A8 Nitrogen adsorption-desorption isotherm of HY zeolite

Table A1 Data from elemental analysis for total nitrogen and sulfur content

Total Nitrogen content

Name	TN (mg)	weight (g)	TN (g/g)	%N
A3M7	0.7329	0.1200	0.0061	0.6108
A5M5	0.9249	0.1200	0.0077	0.7708
A7M3	1.4310	0.1100	0.0130	1.3009
A-HMS	1.5531	0.1100	0.0141	1.4119

Total Sulfur content

Name	Mass of S (g)	Weight (g)	TS (g/g)	%S
M-HMS	0.0105	0.1057	0.0992	9.9243
A3M7	0.0072	0.1008	0.0709	7.0933
A5M5	0.0064	0.1076	0.0599	5.9851
A7M3	0.0033	0.1015	0.0326	3.2640

Table A2 Data from calculation of surface charge of PAC

Sample	pH	Surface charge (C/g)
1	9.78	-21.0795
2	9.63	-7.6424
3	9.51	-3.3454
4	9.47	-1.0167
5	9.38	1.1597
6	9.30	2.8946
7	9.21	4.6074
8	9.08	8.4962
9	8.30	19.7073

Table A3 Data from calculation of surface charge of HMS

Sample	pH	Surface charge (C/g)
1	3.39	20.6894
2	3.6	8.8539
3	3.78	7.3326
4	4.06	2.1769
5	4.37	1.5538
6	4.99	-0.0495
7	5.42	-0.8257
8	5.97	-2.0218
9	6.7	-8.4018
10	7.24	-20.5957
12	8.23	-33.4557
13	8.56	-54.5800
14	8.94	-115.0719

Table A4 Data from calculation of surface charge of A-HMS

Sample	pH	Surface charge (C/g)
1	9.67	-21.6759
2	9.60	-7.6125
3	9.58	-2.9676
4	9.57	-0.6363
5	9.53	1.6316
6	9.51	3.5461
7	9.50	5.3390
8	9.38	9.0818
9	9.38	19.9328

Table A5 Data from calculation of surface charge of M-HMS

Sample	pH	Surface charge (C/g)
1	8.63	-24.0164
2	7.56	-9.5771
3	7.01	-4.7963
4	6.62	-2.3749
5	6.14	-0.0338
6	4.96	1.4146
7	4.40	1.9738
8	3.97	2.5858
9	3.45	2.3544

Table A6 Data from calculation of surface charge of A3M7

Sample	pH	Surface charge (C/g)
1	8.56	-24.2884
2	7.85	-9.4485
3	7.39	-4.7962
4	7.09	-2.4298
5	6.77	-0.0053
6	6.62	1.9320
7	6.41	3.8733
8	6.21	7.7682
9	5.13	18.8340

Table A7 Data from calculation of surface charge of A5M5

Sample	pH	Surface charge (C/g)
1	9.37	-23.4226
2	9.17	-8.9258
3	9.11	-4.3742
4	9.09	-1.8768
5	9.03	0.5108
6	8.90	2.3656
7	8.81	4.2612
8	8.87	8.1223
9	8.57	19.7511

Table A8 Data from calculation of surface charge of A7M3

Sample	pH	Surface charge (C/g)
1	8.76	-23.7093
2	8.52	-9.4174
3	8.37	-4.7039
4	8.38	-2.3164
5	8.3	0.0938
6	8.25	2.0308
7	8.18	3.9713
8	8.08	7.8548
9	7.68	19.3987

Table A9 Data from calculation of surface charge of NaY zeolite

Sample	pH	Surface charge (C/g)
1	9.94	-19.8855
2	9.46	-8.3217
3	9.05	-4.3406
4	8.33	-2.3198
5	7.88	0.0358
6	7.58	1.9625
7	7.31	3.8295
8	7.00	7.6744
9	6.69	19.4079

Table A10 Data from calculation of surface charge of HY zeolite

Sample	pH	Surface charge (C/g)
1	5.17	-24.5451
2	4.88	-10.2392
3	4.74	-5.6718
4	4.65	-3.4958
5	4.61	-1.1773
6	4.54	0.5600
7	4.48	2.3009
8	4.36	5.5794
9	4.05	15.1927

Table A11 Data from calculation of surface charge of Activated alumina

Sample	pH	Surface charge (C/g)
1	9.92	-19.8372
2	9.22	-8.7191
3	7.79	-4.8443
4	7.37	-2.2986
5	7.21	0.0048
6	6.59	1.8787
7	6.32	0.3011
8	5.87	7.4494
9	5.3	19.2128

APPENDIX B

Table B1 Data from Adsorption kinetic of PAC, HMS, A-HMS, M-HMS, A3M7, A5M5, A7M3, NaY, HY and Activated alumina

Time	Concentration of DCAA after adsorption (ppb)									
	PAC	HMS	A-HMS	M-HMS	A3M7	A5M5	A7M3	NaY	HY	Alumina
0	106.92	106.92	106.92	106.92	106.92	106.92	106.92	106.92	106.92	106.92
0.17	54.25	-	-	-	-	-	-	-	-	-
0.33	44.92	-	-	-	-	-	-	-	-	-
0.5	39.28	95.35	103.20	100.62	98.05	95.58	94.38	107.15	96.23	95.66
1	37.96	91.90	95.67	100.19	97.20	94.16	93.45	97.83	90.35	95.59
3	37.94	91.59	95.22	92.82	88.72	93.77	87.26	96.11	87.18	94.29
6	36.63	90.29	90.40	-	85.06	85.84	90.02	86.90	84.00	91.81
12	37.12	-	-	87.88	87.63	90.01	83.24	82.77	84.34	82.67
24	29.72	82.64	95.32	91.54	82.03	92.65	90.09	-	-	-
48	28.76	87.86	95.13	90.16	86.21	93.96	91.75	86.57	87.56	86.73
72	29.86	91.12	99.64	93.26	91.70	94.49	93.40	89.55	90.66	89.95

Table B2 Data from Adsorption isotherm of PAC, HMS, A-HMS, M-HMS, A3M7, A5M5, A7M3, NaY, HY and Activated alumina at pH 7

Initial concentration (µg/l)	Adsorption capacity of DCAA (µg/g)									
	PAC	HMS	A-HMS	M-HMS	A3M7	A5M5	A7M3	NaY	HY	Alumina
10	2.59	0.01	0.58	0.76	0.63	0.06	1.00	0.04	0.84	0.08
30	11.04	8.05	3.43	5.21	-	2.57	-	-	-	-
60	21.44	8.74	4.19	8.41	2.76	4.05	7.33	1.80	3.84	3.32
100	35.08	16.92	9.24	15.30	8.49	7.47	17.11	3.41	5.79	6.99
150	57.24	27.91	13.88	23.64	-	15.82	-	9.33	13.28	13.44
200	69.38	31.03	19.75	29.53	10.49	18.12	28.42	11.18	10.48	16.21
300	109.01	49.79	27.05	39.26	20.23	35.79	35.05	13.95	21.51	28.19

Table B3 Data from Adsorption isotherm of PAC, HMS, A-HMS, M-HMS, A3M7, A5M5, A7M3, NaY, HY and Activated alumina at pH 5

Initial concentration (µg/l)	Adsorption capacity of DCAA (µg/g)									
	PAC	HMS	A-HMS	M-HMS	A3M7	A5M5	A7M3	NaY	HY	Alumina
10	3.96	0.98	0.90	1.59	1.62	0.75	0.73	0.11	1.95	2.79
60	29.63	5.55	4.75	10.29	8.63	5.07	6.08	2.80	10.81	12.04
120	50.02	11.18	10.63	18.82	9.86	10.89	12.18	4.27	15.92	15.06
180	71.29	20.36	16.98	30.80	25.85	16.17	19.89	14.19	25.05	29.55
300	130.87	32.27	24.77	40.30	34.70	31.89	34.92	27.54	41.27	41.65

Table B4 Data from Adsorption isotherm of PAC, HMS, A-HMS, M-HMS, A3M7, A5M5, A7M3, NaY, HY and Activated alumina at pH 9

Initial concentration (µg/l)	Adsorption capacity of DCAA (µg/g)									
	PAC	HMS	A-HMS	M-HMS	A3M7	A5M5	A7M3	NaY	HY	Alumina
10	2.50	0.73	0.53	0.26	0.24	0.37	0.82	0.03	0.06	-0.26
60	3.93	2.42	2.66	1.47	-1.84	2.78	-1.86	-2.02	1.15	1.80
120	5.01	9.22	3.53	9.30	5.36	7.20	5.24	3.35	6.24	9.31
180	9.30	14.84	12.71	17.18	10.95	16.65	13.11	5.69	14.38	16.07
300	7.34	33.38	22.20	20.05	20.99	22.61	26.06	7.25	22.74	20.44

Table B5 Data from Adsorption isotherm of PAC, HMS, NaY zeolite and Activated alumina at 40°C

Initial concentration (µg/l)	Adsorption capacity of DCAA (µg/g)			
	PAC	HMS	NaY	Alumina
10	2.79	1.40	0.56	1.13
60	18.71	6.87	7.15	5.25
120	39.12	15.56	14.77	10.52
180	63.89	23.87	26.39	14.06
300	82.68	39.94	29.88	13.11

Table B6 Data from Adsorption isotherm of PAC, HMS, NaY zeolite and Activated alumina at 60°C

Initial concentration (µg/l)	Adsorption capacity of DCAA (µg/g)			
	PAC	HMS	NaY	Alumina
10	2.35	0.72	0.22	0.12
60	14.92	5.13	6.13	3.50
120	30.82	15.10	13.39	8.83
180	52.24	24.81	21.03	17.41
300	72.55	36.44	26.76	15.49
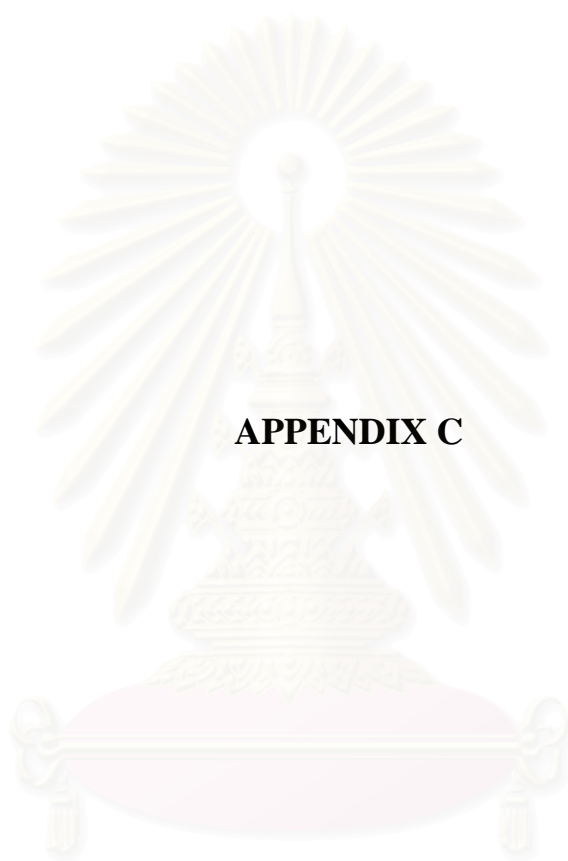
APPENDIX C

Table C1 Estimated calculation of cost for HMS synthesis

Materials and Energy	Cost (baht)
1. Incinerator	59
2. Magnetic stirrer	39
3. TEOS	23
4. Dodecylamine	20
5. Ethanol	16
Total	**157**

* Total amount of HMS per one batch = 7.5 g

BIOGRAPHY

Mr. Suwat Soonglerdsongpha was born on June 3, 1983 in Chonburi province. After he graduated high school in Banglamung, Chonburi, he went to study in Faculty of science at King Mongkut's Institute of Technology Ladkrabang (KMIT'L). He graduated Bachelor's degree of Science in Environmental Resource Chemistry in 2005. After that he continued his study for a Master's Degree of Science in Environmental Management (International program) at Chulalongkorn University in May, 2005.